Cerebral Cortex March 2015;25:788–805
doi:10.1093/cercor/bht278
Advance Access publication October 9, 2013

Morphological and Physiological Characterization of Pyramidal Neuron Subtypes in Rat Medial Prefrontal Cortex

Karlijn I. van Aerde[1,4] and Dirk Feldmeyer[1,2,3]

[1]Forschungszentrum Jülich, Institute of Neuroscience and Medicine, INM-2, D-52425 Jülich, Germany, [2]Department of Psychiatry, Psychotherapy and Psychosomatics, RWTH Aachen University, Medical School, D-52074 Aachen, Germany and [3]Jülich Aachen Research Alliance, Translational Brain Medicine (JARA-Brain), D-52074 Aachen, Germany [4]Current address: Netherlands Institute for Neuroscience, Royal Netherlands Academy of Arts and Science, 1105 BA Amsterdam, The Netherlands

Address correspondence to Dirk Feldmeyer, Institute of Neuroscience and Medicine, INM-2, Forschungszentrum Jülich, Leo-Brandt-Straße, D-52425 Jülich, Germany. Email: d.feldmeyer@fz-juelich.de

The medial prefrontal cortex (mPFC) has been implicated in cognitive and executive processes including decision making, working memory and behavioral flexibility. Cortical processing depends on the interaction between distinct neuronal cell types in different cortical layers. To better understand cortical processing in the rat mPFC, we studied the diversity of pyramidal neurons using in vitro whole-cell patch clamp recordings and biocytin staining of neurons, followed by morphological analysis. Using unsupervised cluster analysis for the objective grouping of neurons, we identified more than 10 different pyramidal subtypes spread across the different cortical layers. Layer 2 pyramidal neurons possessed a unique morphology with wide apical dendritic field spans and a narrow basal field span. Layer 3 contained the only subtype that showed a burst of action potentials upon current injection. Layer 5 pyramidal neurons showed the largest voltage sags. Finally, pyramidal neurons in layer 6 (L6) showed a great variety in their morphology with 39% of L6 neurons possessing tall apical dendrites that extend into layer 1. Future experiments on the functional role of the mPFC should take into account the great diversity of pyramidal neurons.

Keywords: 3D reconstructions, classification, cluster analysis, heterogeneity, layers, patch clamp

Introduction

The medial prefrontal cortex (mPFC) is important for several cognitive and executive processes such as attention, decision making, working memory, and behavioral flexibility (Goldman-Rakic 1995; Fuster 2000, 2001; Miller 2000; Ragozzino 2007). The mPFC of rodents consists of several areas including the prelimbic and infralimbic cortices (Van Eden and Uylings 1985; Uylings et al. 2003; Hoover and Vertes 2007). The prelimbic cortex is involved in behavioral flexibility (Marquis et al. 2007; Ragozzino 2007), whereas the infralimbic cortex seems to be involved in impulse behavior and habit formation (Chudasama et al. 2003; Killcross and Coutureau 2003; Murphy et al. 2005). Dysfunction of the prefrontal cortex, resulting from sleep deprivation or pathological conditions like schizophrenia, can result in cognitive malfunctions such as attention deficits and decreased working memory, behavioral preservation or stereotypy, increased irritability, and apathy (Broersen et al. 1995; Yang et al. 1999; Harrison et al. 2000; Muzur et al. 2002; Ragozzino 2007; Van Der Werf et al. 2009).

Cortical processing depends on the interaction between distinct neuronal cell types in different cortical layers and areas. Pyramidal neurons in the main output layer of the neocortex, layer 5 (L5), have been studied most extensively at the functional and structural levels. These studies have revealed differences in subcortical projection areas of different pyramidal cell subtypes as well as differences in intralaminar connections, suggesting that they can form subnetworks depending on pyramidal cell type (Molnar and Cheung 2006; Wang et al. 2006; Otsuka and Kawaguchi 2008; Brown and Hestrin 2009; Dembrow et al. 2010). In addition, pyramidal cell subtypes, like interneurons, are differentially affected by neuromodulators such as acetylcholine, noradrenaline, serotonin, and adenosine (Beique et al. 2007; Couey et al. 2007; Eggermann and Feldmeyer 2009; Dembrow et al. 2010; Poorthuis et al. 2013; Van Aerde et al. 2013).

Cortical circuit organization has been studied predominantly in sensory cortices such as the visual and somatosensory cortices. These studies have led to a serial model of cortical circuit organization whereby the main thalamic input to layer 4 (L4) is forwarded to supragranular layer 2/3 (L2/3). Here, it is integrated with input from other cortical areas (Feldmeyer et al. 2002; Douglas and Martin 2004; Schubert et al. 2007; Feldmeyer 2012; Oberlaender et al. 2012). The resulting activity is then relayed to output L5 pyramidal neurons that drive subcortical structures involved in action, like the basal ganglia. L5 neurons also innervate L6 pyramidal neurons that feedback to the thalamus, and thus influence the synaptic input to the neocortex. Several shortcuts in this circuit have also been identified such as direct connections from L4 to L5A (Feldmeyer et al. 2005). How cortical circuits are organized in agranular cortices like the prefrontal cortex, which lack a granular L4, is less clear (Shepherd 2009; Hooks et al. 2011).

To better understand signal processing in the prefrontal cortex, it is essential to identify the different neuronal elements forming the cortical microcircuit. In this study, we probed the diversity of pyramidal neuron subtypes that are present in the rat mPFC. Although a certain level of similarity to sensory cortices can be expected, the agranular character and the unique functional role of the mPFC is likely reflected in a unique neuronal network. Indeed, it is estimated that pyramidal neurons in the prefrontal cortex have on average up to 23 times more dendritic spines than those in the visual cortex (Elston 2003).

To study the functional and structural diversity of pyramidal neurons throughout all cortical layers of the mPFC, we made whole-cell patch clamp recordings and simultaneous biocytin fillings in rat brain slices. Post hoc staining of the labelled neurons and 3D reconstructions provided a basis for morphological analysis of the neurons. Subsequently, we used an unsupervised cluster analysis (CA) based on physiological and

morphological parameters to classify pyramidal neurons. So far, an objective classification like the one described in this study, including an extensive morphological analysis, has not been performed for pyramidal neurons in the mPFC. Moreover, because recording conditions were identical for neurons recorded in different layers, we were able to pinpoint the unique characteristics of pyramidal cells in each cortical layer. We found that broad tufted regular spiking (RS) neurons in L5 are the most distinct subtype in the rat PFC. L2 pyramidal neurons were unique in their morphology, being the only cell type where the field span of its apical dendrites was much larger than that of its basal dendrites. L3 contained the only subtype that responded to a depolarizing current injection with a burst of action potentials (APs). Finally, L6 pyramidal neurons showed a great variety in their morphology. Typical for the mPFC seems to be that a high percentage of them have apical dendrites that ascend to Layer 1 (L1). The distinction between pyramidal subtypes is important for understanding cortical processing in the mPFC. Indeed, we found in our accompanying article that the neuromodulator adenosine exerts differential effects depending on pyramidal cell subtype (Van Aerde et al. 2013).

Materials and Methods

Slice Preparation

All experimental procedures were carried out in accordance with the German Animal Welfare Act, the European Directive on the Protection of Animals used for Scientific Purposes, and the guidelines of the Federation of European Laboratory Animal Science Association.

Wistar rats (Charles River, either sex) aged 24–46 postnatal days (P24–46) were anesthetized with isoflurane and decapitated, their brains were quickly removed, and placed in ice-cold artificial cerebrospinal fluid (ACSF) containing: 125 mM NaCl, 2.5 mM KCl, 1.25 mM NaH_2PO_4, 5 mM $MgSO_4$, 1 mM $CaCl_2$, 25 mM $NaHCO_3$, 25 mM glucose, 3 mM Myo-Inositol, 2 mM Na-pyruvate, and 0.4 mM vitamin C (300 mOsm).

For prefrontal cortical slices, coronal sections (350 µm) of the prelimbic mPFC were cut in ice-cold ACSF solution bubbled with carbogen gas (95% O_2/5% CO_2) using a MICROM vibratome slicer (Walldorf, Germany). For older animals (>P35), a sucrose-based slicing solution was used containing: 206 mM sucrose, 2.5 mM KCl, 1.25 mM NaH_2PO_4, 3 mM $MgSO_4$, 1 mM $CaCl_2$, 25 mM $NaHCO_3$, and 25 mM glucose (300 mOsm).

Slices were then transferred to a holding chamber placed in a water bath at 35 °C and left to recover for at least 1 h; subsequently, the water bath was allowed to cool down to room temperature. Slices were stored for up to 8 h in ACSF containing: 125 mM NaCl, 2.5 mM KCl, 1.25 mM NaH_2PO_4, 1 mM $MgSO_4$, 2 mM $CaCl_2$, 25 mM $NaHCO_3$, and 25 mM glucose, bubbled with carbogen gas (95% O_2/5% CO_2).

Electrophysiology

Pyramidal cells, visualized using infrared differential interference contrast microscopy, were selected on the basis of their morphology and firing pattern. All experiments were performed at 30 ± 1 °C. This recording temperature was chosen to limit the decrease in oxygenation that occurs at higher temperatures. Basic cell passive and active properties were assessed by initial hyperpolarizations, followed by stepped depolarizations.

Recordings were made using an EPC10 amplifier (HEKA, Lambrecht, Germany). Signals were sampled at 10 kHz, filtered at 2.9 kHz using Patchmaster software (HEKA), and later analyzed off-line (Igor Pro software, Wavemetrics, Lake Oswego, OR, USA).

Patch pipettes (4–8 MΩ) were pulled from thick-wall borosilicate capillaries (outer diameter: 2 mm; inner diameter: 1 mm) and filled with intracellular solution containing 135 mM K-gluconate, 4 mM KCl, 10 mM HEPES, 10 mM Na-phosphocreatine, 4 mM ATP-Mg, and 0.3 mM GTP-Na (pH adjusted to 7.3 with KOH; osmolarity, ~300 mOsm). Biocytin at a concentration of 3–5 mg/mL was added to the internal solution (Sigma-Aldrich, Steinheim, Germany).

Whole-cell series resistance was on average 29.6 ± 8.9 MΩ (mean ± SD, $n = 108$) and was compensated by 80%. Neurons were excluded from the analysis when their series resistance was larger than 50 MΩ or changed by more than 25% during an experiment.

Histological Procedures

After intracellular recording, the slices were fixed in 4% paraformaldehyde in 0.1 M phosphate buffer (PB; pH 7.4) for at least 24 h, followed by several rinses with PB. Then slices were treated with 1% H_2O_2 in PB for 10 min, to reduce endogenous peroxidase activity. Biocytin-filled cells were visualized using avidin-biotinylated horseradish peroxidase complex reaction (ABC-Elite; Camon, Wiesbaden, Germany) with 3,3′-diaminobenzidine (Sigma-Aldrich, St. Louis, MO, USA) as chromogen giving a dark reaction product. After dehydration and embedding in Moviol (Clariant, Sulzbach, Germany) or in Eukitt (Marienfeld Lab. Glassware, Lauda-Königshof, Germany), neurons were reconstructed using NEUROLUCIDA® software (MBF Bioscience) at 1000-fold magnification (Radnikow et al. 2012; Marx et al. 2012).

Data Analysis

Electrophysiological data were analyzed using custom-written procedures in Igor Pro 6.0 (Wavemetrics).

Passive Cell Properties and Spike-Time Adaptation

The input resistance (R_{in}) was calculated as the slope of the linear fit between −60 to −70 mV of the current–voltage (*I–V*) relationship. The membrane time constant (τ_m) was estimated with a mono-exponential fit of the voltage response after a current step of −50 pA. The voltage sag was the percentage difference between the initial and sustained response upon 1 s current injections that would cause a hyperpolarization of approximately −7.5 mV. Rheobase current, the minimal current that elicited an AP, was determined using a small step size of 10 pA.

Spike-time adaptation is shown for the current step when at least 10 APs were elicited. We took the approach of comparing neurons with approximately the same number of APs instead of the response to the same amount of current injection, because individual differences in rheobase current and R_{in} would lead to a highly variable number of elicited APs with a fixed current injection. Although spike-time adaptation was similar for individual neurons for current steps that elicited more than ~7 APs, especially the first interspike interval was variable for lower current injections when <7 APs were elicited. RS and adapting neurons showed a tendency to develop a faster first interspike interval (ISI), or doublet, only upon higher current injections when more than 5 APs were elicited. This is in stark contrast to initial bursting neurons which generally displayed an even faster doublet already at the rheobase current. Because the variation between neurons was largest for the ratio with the first 3 interspike intervals, we selected these parameters for an unsupervised CA to group the pyramidal neurons.

The slope of the input–output relation (i.e., firing rate (*F*) as a function of current injection (*I*)) was calculated with a linear fit between 0 and 300 pA. This limitation was necessary for 2 reasons: 1) Not all neurons were injected with higher current values, and 2) L3 bursting neurons typically showed a nonlinear *F–I* relationships: Initially, firing rates increased only slowly, followed by a steeper slope at higher current injections. Because the initial slope was different for the L3 subtypes, we limited our analysis to the initial part.

Morphology

Neurons were three-dimensionally reconstructed using NEUROLUCIDA® software (MBF Bioscience). The field span of apical and basal dendrites was defined as the widest distance between apical or basal dendrites, measured parallel to the pia. Other morphological parameters such as total dendritic length, number of branches, and soma

size were analyzed with NEUROEXPLORER® software (MBF Bioscience). The soma size was calculated as the maximal soma circumference from the projection in the 2D plane.

For L3 pyramidal neurons that could have more or less extensive oblique side branches originating in L3, which could make up a considerable part of the total sums for slender tufted neurons, we included only measurements from L1: Field span in L1, combined total length in L1, and number of branches in L1.

Definition of Cortical Layers

The definition of layer borders is important for the identification and proper classification of mPFC pyramidal cells. Layer borders were drawn under low light microscopic magnification conditions using enhanced contrast. Embedding of slices in Eukitt (see above) prevented fading of cytoarchitectural features and improved the contrast between layers considerably (Marx et al. 2012). Layer borders were defined based on cytoarchitectural features of which cell density and cell soma size were most important in agreement with earlier studies of the prefrontal cortex (Van Eden and Uylings 1985; Gabbott et al. 1997; Gabbott et al. 2005). In acute prelimbic cortex slices, L2 is clearly distinguishable from L1 and L3 as a thin dark band that is densely packed with neuron somata. L2 is situated directly beneath L1, which is almost devoid of neurons apart from a few interneuron types that are dispersed between dendrites and axon collaterals (Fig. 1*A*). After fixation, the difference in cell density between L2 and L3 is still visible (see, e.g., Fig. 5*B*,*C*). L2 is the thinnest layer of the prefrontal cortex containing only a few "rows" of pyramidal neurons. L3 is about 2–3 times wider than L2 and has about the same width as L1 (Van Eden and Uylings 1985; Gabbott et al. 1997, 2005). L1 is particularly wide in the prefrontal cortex compared with other cortical regions. Because rodents lack a L4 in some cortical areas including the mPFC (Uylings and Van Eden 1990; Uylings et al. 2003), L3 borders directly on L5. The border between L3 and L5 was based on the difference in cell soma size between L3 and L5 neurons (Table 2 and Supplementary Fig. 1). In the acute slice, this difference in soma size can be best seen under high magnification (×40 objective). After fixation and embedding in Eukitt, this border is clearly discernible under low magnification (×4 objective, Fig. 5*B*,*C*). L5 comprises roughly the middle third of the prelimbic cortex. Although at the macroscopic level, some indications can be seen for a subdivision of L5 in a superficial L5A and a deep L5B, this is not as clearly discernible as in sensory cortical areas like the somatosensory cortex (Feldmeyer et al. 2005; Schubert et al. 2006). Therefore, we did not subdivide L5 into different sublaminae. Layer 6 (L6) comprises the lower third of the cortex (Van Eden and Uylings 1985; Gabbott et al. 1997, 2005). The border between L5 and L6 is expected to be approximately halfway of the distance between the border of L3–L5 and the border of L6 with the white matter. In the acute slice, the difference in soma size marks the difference between L5 and L6 pyramidal neurons (Table 2 and Supplementary Fig. 1). In addition, in contrast to L5 pyramidal neurons that all have ascending apical dendrites pointing towards the pia, L6 neurons often show oblique, horizontally orientated or inverted main dendrites. Although the main dendrite cannot be followed far in the acute slice, the departure and thus the orientation of the main dendrite with respect to the pial surface, is often clearly visible. After fixation, the border between L5 and L6 in the mPFC is much more difficult to identify. In primary sensory cortices, L6 can be subdivided in L6A and L6B (Tömböl 1984; Valverde

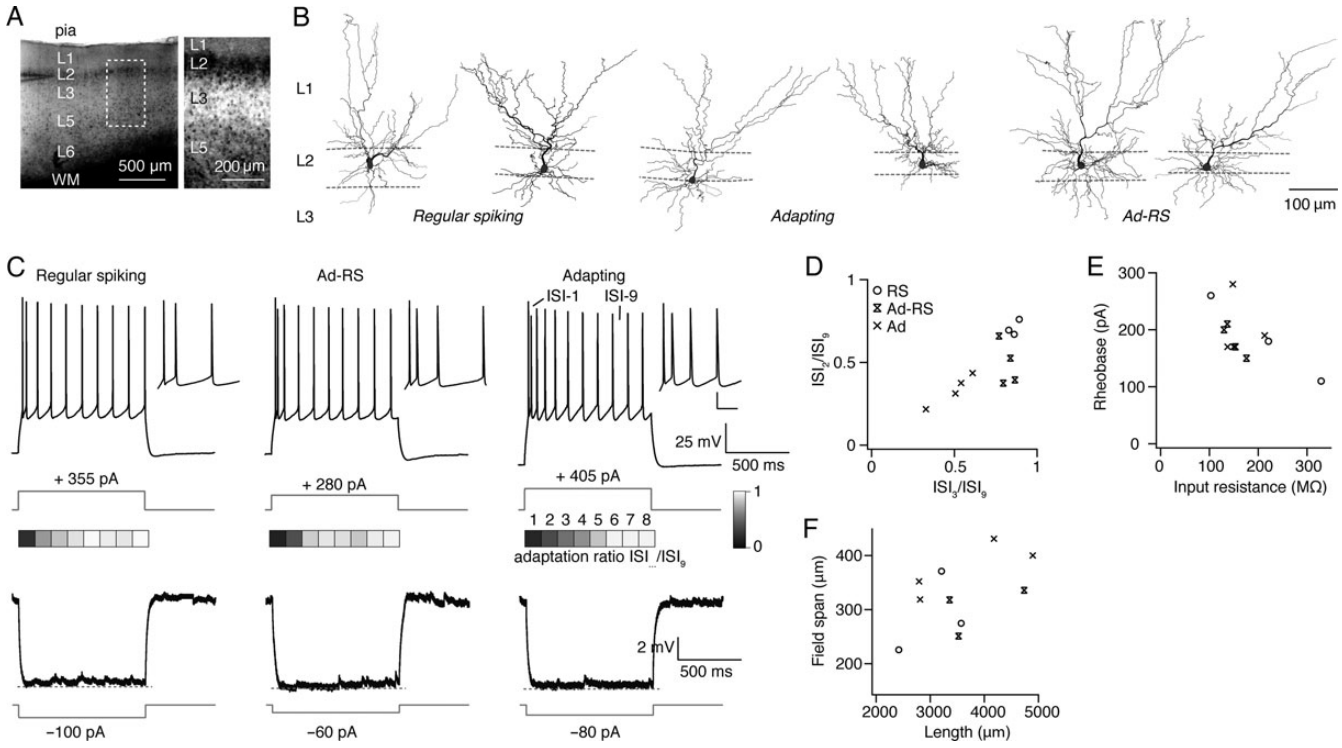

Figure 1. L2 pyramidal neurons. (*A*) Left, DIC image at low magnification where pia, successive layers (L) and white matter (WM) are indicated. Note the patch pipette in left layer 2. Right, DIC image from another brain slice at higher magnification (comparable to the boxed region at the left) where layers can be particularly well recognized. (*B*) Morphological reconstruction of soma and dendrites from L2 pyramidal neurons. Note the large span width of apical dendrites compared with basal dendrites, and the asymmetric apical dendrite tree in some neurons. (*C*) Electrophysiological profile of a regular spiking neuron (RS, left), an adapting neuron (Ad, right), and an intermediate neuron (Ad-RS, middle): The upper panel shows the response when a minimum of 10 action potentials were elicited with the corresponding current step in gray. The inset shows a magnification of the first spikes (scale bar: 20 mV, 50 ms). Below, adaptation ratios from interspike interval 1–8 with the 9th interspike interval (ISI-9) are shown in color code, that is, the ratio between the first ISI (ISI-1) and ISI-9 is shown at the most left, followed by the ratio between ISI-2 and ISI-9 and so forth. The lower panel shows the response to a negative current step (gray, bottom) that would lead to an ~−7.5 mV hyperpolarization of the membrane potential. Current steps are indicated below. Note the virtual absence of a voltage sag in these neurons. (*D*) Ratio of ISI-2 to ISI-9 and ISI-3 to ISI-9 shows a continuum of responses between regular spiking (RS, circles, $n = 3$) and adapting (Ad, crosses, $n = 4$) pyramidal neurons (Ad-RS, hourglass, $n = 4$). (*E*) Subtypes defined by spike timing are not different for passive physiological properties (legend as in *D*). (*F*) Subtypes defined by spike timing are not different for morphological properties (legend as in *D*).

et al. 1989; Marx and Feldmeyer 2012). We did not observe such a clear sublamination in L6 in the mPFC at the macroscopic level. However, as our recordings were made primarily in the upper two-thirds of L6, the majority of the neurons described here are most likely L6A pyramidal neurons.

Cluster Analysis and Statistics

Data are represented as mean ± standard error of the mean (SEM). Statistical analysis used either the unpaired Student's *t*-test or ANOVA test for multiple comparisons, followed by a post hoc Tukey test or a Student Newman–Keuls test when more than 3 groups were compared. Correlation analysis was performed by calculating Pearson correlation coefficients. Unsupervised CA was performed using Euclidean distances and the Ward method. The final number of clusters was suggested by the Thorndike procedure, where the maximal derivative of the sorted linkage distances was taken as cutoff value (Thorndike 1953). Each parameter was normalized as min–max normalization. Principal component analysis (PCA) was used to eliminate correlated variables to avoid double weighting or misinterpretation of the CA (data not shown). Parameters that were often, but not always, contributing in a similar way to the PCA were the ratio of ISI_1/ISI_9 and ISI_2/ISI_9. Morphological parameters that were often correlated were the total length and number of branches of apical or basal dendrites. Using this approach, we were able to exclude all parameters that were highly correlated from the CA. To eliminate uninformative parameters, the resulting groups or clusters of the CA were then compared for each parameter using ANOVA tests, and the CA was repeated with only those parameters included that showed significant different values between the groups. The resulting parameters that were thus used for the final CA are listed in Table 1 for the different layers.

All statistical tests were performed using XLSTAT software (Addinsoft, Andernach, Germany). Single and double asterisks represent $P < 0.05$ and $P < 0.01$ respectively.

Results

For the classification of different pyramidal subtypes, we recorded 119 pyramidal neurons located throughout L2 to L6 in acute slices of the rat prelimbic cortex, which is part of the rat mPFC. The prelimbic cortex is situated along the midline of the cortex and is bordered by the anterior cingulate cortex and the infralimbic cortex (Paxinos and Watson 2005). After electrophysiological recordings, slices were fixed and processed for staining, and neurons were reconstructed to analyze their morphology. Only neurons with stable resting membrane potentials (RMP) of below −60 mV and with excellent staining of soma and dendrites were used for electrophysiological and morphological data analysis.

Layer 2 Pyramidal Neurons

We recorded from 12 L2 pyramidal neurons, 1 of which was excluded from electrophysiological analysis because the series resistance was too high. Morphologically, L2 pyramidal neurons are unique in the relative field span of their apical and basal dendrites (Table 2; for reconstructions of all L2 neurons, see Supplementary Fig. 2). In contrast to L3 or L5 pyramidal neurons, the field span of the apical dendritic tuft of L2 neurons is much larger than that of basal dendrites (Fig. 1*B*, field span of apical dendrites 339 ± 20 µm, basal dendrites 198 ± 9 µm, $n = 11$, $P < 0.01$). Another prominent feature is a very short apical trunk (measured from the soma to the apical tuft, Fig. 1*B*). Finally, the apical dendritic tree of L2 pyramidal cells is often asymmetric (Fig. 1*B*, most right example). To circumvent the possibility that the asymmetric nature of L2 pyramidal neurons is resulting in a biased measurement of the field span, we determined the total length of the apical dendrite. This parameter is independent of the shape of the apical dendritic tree. L2 neurons have higher total apical dendritic lengths compared with some other subtypes, such as L3 neurons, but it is especially the relation between apical and basal dendrites that sets these neurons apart. Whereas most pyramidal subtypes do not exceed a ratio of about 1:1 for the total length of apical and basal dendrites, and broad tufted L5 neurons have on average 1.5 times more apical dendritic length, L2 and L6 tall neurons have about 2.5 times more apical than basal dendritic length (Table 2). In the case of L2 neurons, this is also reflected in the ratio of apical to basal field span (ratio field span: 1.73 ± 0.09, Table 2). However, as the ratio of field span is less than the ratio of total length, the asymmetric nature of L2 pyramidal neurons does not lead to an overestimation of the size of the apical tree for these neurons.

Table 1
Morphological and electrophysiological parameters that were used for unsupervised cluster analysis (CA)

	Morphological	Electrophysiological	
		Active	Passive
Layer 2 neurons	Field span in L1 (µm) Total length apical Dendrites (µm) Number of apical branches	ISI-1 ISI-3 Increase in firing frequency per 100 pA	RMP (mV) Voltage sag (%) Input resistance (MΩ) Time constant (ms) Rheobase (pA)
Layer 3 neurons	Field span in L1 (µm) Number of apical branches	ISI-2 ISI-3 Increase in firing frequency per 100 pA	RMP (mV) Voltage sag (%) Time constant (ms) Rheobase (pA)
Layer 5 neurons	Field span in L1 (µm) Field span apical dendrite (µm) Total length basal Dendrites (µm) Number of apical branches Number of basal branches	ISI-3	RMP (mV) Voltage sag (%) Input resistance (MΩ) Time constant (ms) Rheobase (pA)
Layer 6 neurons	Field span basal dendrites (µm) Total length apical Dendrites (µm) Total length basal Dendrites (µm) Vertical span apical Dendrite (ending layer)	-	RMP (mV) Voltage sag (%) Input resistance (MΩ) Time constant (ms) Rheobase (pA)

Note: RMP, resting membrane potential; rheobase, minimal current to elicit an action potential.

Table 2
Morphological properties of pyramidal neurons in layer 2–6 (L2–L6) of the rat prefrontal cortex

Layer	2	3				5			5/6	6		
Subclass	L2	L3 RS	L3 broad Ad	L3 bursting	L3 slender Ad	L5 slender LR	L5 slender HR	L5 RS	L5 wide	L6 tall	L6 small	L6 short
n	11	7	4	6	3	30	11	18	4	5	5	5
Location within cortex	19 ± 2%	22 ± 2%	26 ± 1%	31 ± 2%	32 ± 3%	48 ± 2%	53 ± 4%	52 ± 2%	64 ± 9%	77 ± 1%	77 ± 4%	85 ± 5%
Vertical span apical dendrite (ending layer)	1.0 ± 0.0	1.0 ± 0.0	1.0 ± 0.0	1.0 ± 0.0	1.0 ± 0.0	1.0 ± 0.0	1.3 ± 0.2	1.0 ± 0.0	1.5 ± 0.5	1.0 ± 0.0	**5.2 ± 0.2**$^{*/**}$	**4.6 ± 0.7**$^{*/**}$
Field span apical dendrite	339 ± 20	259 ± 13	312 ± 14	220 ± 17	228 ± 14	290 ± 17	295 ± 30	**482 ± 24**$^{*/**}$	246 ± 83	295 ± 27	147 ± 10	361 ± 127
Field span apical tuft	339 ± 20	259 ± 13	312 ± 14	193 ± 20	228 ± 14	180 ± 17	228 ± 36	**480 ± 25**$^{*/**}$	246 ± 83	121 ± 48	60 ± 19	327 ± 143
Field span basal dendrite	198 ± 9	249 ± 14	270 ± 19	276 ± 13	253 ± 26	**399 ± 10***	324 ± 21	325 ± 9	**884 ± 81****	215 ± 8	181 ± 8	300 ± 10
Ratio field span tuft/basal	**1.73 ± 0.09**$^{*/**,a}$	1.05 ± 0.06	1.16 ± 0.03	0.71 ± 0.08	0.93 ± 0.16	0.46 ± 0.04	0.73 ± 0.12	1.49 ± 0.08	0.29 ± 0.10	0.58 ± 0.25	0.33 ± 0.10	1.08 ± 0.48
Total length apical dendrite	3531 ± 236	3128 ± 138	2606 ± 47	2008 ± 177	1776 ± 258	3161 ± 115	3471 ± 511	**6530 ± 310****	1757 ± 190	3853 ± 371	1083 ± 144	2470 ± 533
Total length basal dendrite	1649 ± 153	2791 ± 234	2609 ± 330	3123 ± 248	2596 ± 339	**5213 ± 221**$^{*/**}$	3355 ± 274	**4580 ± 220**$^{*/**}$	3074 ± 177	1685 ± 250	1597 ± 131	2464 ± 187
Ratio length	**2.43 ± 0.39****	1.16 ± 0.09	1.07 ± 0.19	0.69 ± 0.13	0.72 ± 0.15	0.64 ± 0.04	1.07 ± 0.14	1.49 ± 0.10	0.57 ± 0.04	**2.52 ± 0.48****	0.72 ± 0.14	1.07 ± 0.27
Sum length	5180 ± 265	5919 ± 308	5215 ± 315	5130 ± 154	4372 ± 324	**8373 ± 220****	6826 ± 667	**11110 ± 368****	4830 ± 358	5538 ± 469	2680 ± 73	4934 ± 437
Soma size (μm^2)	204 ± 7	188 ± 9	178 ± 14	193 ± 20	**294 ± 18****	**292 ± 11****	**311 ± 18**$^{*/**}$	**361 ± 19****	188 ± 18	186 ± 20	185 ± 9	218 ± 24
Number of apical braches	**29 ± 2**^{**,b}	19 ± 2	16 ± 1	11 ± 1	10 ± 2	17 ± 1	20 ± 3	**38 ± 2****	10 ± 3	25 ± 3	14 ± 2	15 ± 5
Number of basal branches	20 ± 2	26 ± 1	24 ± 3	24 ± 3	22 ± 2	31 ± 1	23 ± 2	**37 ± 2****	14 ± 1	20 ± 3	18 ± 3	21 ± 4
Total number of branches	49 ± 3	45 ± 1	39 ± 5	35 ± 2	31 ± 1	48 ± 1	43 ± 4	**75 ± 2****	24 ± 3	45 ± 4	32 ± 2	36 ± 4

Note: [a]L2 is different from all other subtypes with the exception of L5 RS neurons ($P = 0.09$).
[b]L2 is different from all other subtypes with the exception of L6 tall neurons ($P = 0.23$).
For clarity, the results of the post hoc comparison of groups is only given (values in bold followed with asterisks) when a cell type is different from all other cell types, unless otherwise specified. $^{*}P < 0.05$, $^{**}P < 0.01$.

Instead, this suggests that L2 pyramidal neurons have particularly dense apical trees. This is indeed reflected in the high number of apical branches which is higher than for other pyramidal subtypes with the exception of broad tufted L5 neurons (Table 2).

Electrophysiologically, the AP firing pattern of pyramidal neurons varied in response to current injection. L2 pyramidal neurons displayed a continuum of firing patterns that ranged from RS to adapting patterns (Fig. 1*C*,*D*). Of note is that all L2 pyramidal neurons showed a relatively hyperpolarized RMP of -76.5 ± 1.3 ($P < 0.05$ compared with other layers, Table 3) and virtually lacked a voltage sag following a hyperpolarizing current step, indicating low expression, or even absence, of hyperpolarization-activated cyclic nucleotide-gated (HCN) channels in L2 pyramidal neurons (Fig. 1*C* bottom and Table 3). The high rheobase value indicated a particularly low excitability for these cells ($P < 0.01$ in comparison with L5 or L6 pyramidal neurons, Table 3).

The firing pattern of L2 pyramidal neurons were not correlated to the passive properties of these neurons such as the RMP, membrane time constant (τ_m), cellular input resistance (R_{in}), or the rheobase current (minimal current to elicit an AP, Fig. 1*E* and Table 4). Likewise, there was no correlation with morphological parameters such as the field span, the total length, and the number of branches of apical and basal dendrites (Fig. 1*F* and Table 4). In addition, categorizations based on passive physiological properties or morphological properties resulted in subtypes that were similar in other parameters (Supplementary Tables 1 and 2).

To summarize, the high ratio of the apical to basal field span, as well as the ratio of the apical to basal dendritic length are unique for L2 pyramidal neurons (Table 2). It appears that there is no correlation between active and passive physiological properties, or between the morphology and electrophysiology of L2 pyramidal neurons. Subclasses based on these different parameter sets did not overlap substantially, suggesting that L2 neurons are rather homogenous, and that small differences in physiological or morphological parameters do not seem to correspond to different subtypes.

Layer 3 Pyramidal Neurons

To investigate the diversity of L3 pyramidal neurons, we randomly patched 24 pyramidal neurons in this layer (see Supplementary Fig. 3 for reconstructions of all L3 pyramidal neurons). Two of those were excluded from the electrophysiological analysis, and 1 neuron was stained insufficiently. L3 pyramidal neurons were found to be highly diverse in their electrophysiological properties. Apart from RS and adapting neurons, a subpopulation of L3 pyramidal neurons responded with bursts of APs after electrical stimulation (Fig. 2*A*). This bursting behavior was not seen in pyramidal neurons from any other layer of the mPFC. Bursting neurons typically had a nonlinear input–output relationship with an initial shallow rising phase in the firing rate that become markedly stronger upon increased current stimulation (Fig. 2*A*, bottom). We therefore used the initial part of the slope of the firing rate curve as a parameter for the CA. Other parameters that were used are listed in Table 1.

All L3 pyramidal neurons showed prominent apical dendrites that bifurcated in L1. Unsupervised CA of morphological properties of L3 neurons divided these neurons in broad and

Table 3
Electrophysiological properties of pyramidal neurons in layer 2–6 (L2–L6) of the rat prefrontal cortex

Layer	2	3				5			5/6	6		
Subclass	L2	L3 RS	L3 broad Ad	L3 bursting	L3 slender Ad	L5 slender LR	L5 slender HR	L5 RS	L5 wide	L6 tall	L6 small	L6 short
n	10	7	4	7	3	30	11	18	4	4	2	4
ISI-1/ISI-9	0.22 ± 0.03	0.19 ± 0.04	0.11 ± 0.01	0.09 ± 0.02	0.11 ± 0.02	0.21 ± 0.02	0.27 ± 0.03	0.22 ± 0.02	0.31 ± 0.11	0.46 ± 0.07	**1.06 ± 0.42****	0.42 ± 0.12
ISI-2/ISI-9	0.52 ± 0.05	0.46 ± 0.09	0.28 ± 0.03	0.15 ± 0.03	0.21 ± 0.04	0.43 ± 0.03	0.50 ± 0.04	0.79 ± 0.04	0.46 ± 0.14	0.75 ± 0.11	**1.28 ± 0.39****	0.66 ± 0.19
ISI-3/ISI-9	0.75 ± 0.05	0.71 ± 0.09	0.53 ± 0.04	**0.23 ± 0.05****,a	0.33 ± 0.06	0.61 ± 0.03	0.67 ± 0.05	0.91 ± 0.02	0.64 ± 0.12	0.86 ± 0.10	**1.35 ± 0.20****,b	1.12 ± 0.14
Increase firing rate (Hz/100 pA)	6.2 ± 0.5	6.2 ± 0.7	8.0 ± 1.0	1.3 ± 0.2	5.7 ± 0.4	5.6 ± 0.3	7.0 ± 0.7	6.4 ± 0.2	10.2 ± 2.6	**15.6 ± 1.5***/**	**20.8 ± 5.2****	11.6 ± 1.8
RMP (mV)	−76.0 ± 1.3	−79.2 ± 0.8	−71.5 ± 1.9	−66.5 ± 0.9	−66.3 ± 0.6	−67.4 ± 0.5	−65.4 ± 0.9	−64.0 ± 0.7	−66.4 ± 2.0	−68.1 ± 1.9	−76.1 ± 1.3	−75.2 ± 2.9
Voltage sag (%)	3.0 ± 0.8	0.3 ± 0.3	3.0 ± 1.4	11.0 ± 1.5	15.3 ± 4.0	14.1 ± 1.4	14.0 ± 2.1	**23.8 ± 1.7***/**	10.6 ± 3.3	10.3 ± 2.5	6.9 ± 1.4	4.4 ± 2.5
Input resistance (MΩ)	175 ± 21	143 ± 9	185 ± 9	138 ± 11	172 ± 31	144 ± 6	249 ± 22	90 ± 5	**365 ± 49****	276 ± 47	**433 ± 40****	236 ± 18
Time constant (ms)	20.1 ± 1.2	18.4 ± 0.5	27.1 ± 2.7	29.1 ± 2.0	31.9 ± 7.9	31.7 ± 1.3	41.7 ± 2.3	21.2 ± 1.0	33.6 ± 2.9	29.7 ± 4.0	21.8 ± 5.5	21.4 ± 4.7
Rheobase (pA)	**181 ± 12***/**	**244 ± 11***/**	115 ± 16	120 ± 10	93 ± 23	123 ± 7	67 ± 4	**179 ± 10***/**	53 ± 6	78 ± 22	65 ± 5	125 ± 23

Note: [a]L3 bursting neurons are different from all other subtypes with the exception of L3 slender tufted adapting neurons ($P = 0.41$).
[b]L6 small neurons are different from all other subtypes with the exception of L6 short neurons ($P = 0.12$).
For clarity, the results of the post hoc comparison of groups is only given (values in bold followed with asterisks) when a cell type is different from all other cell types, unless otherwise specified. *$P < 0.05$, **$P < 0.01$.

slender tufted neurons (Fig. 2*B* and Supplementary Table 4). Two neurons with more extensive basal dendrites were classified as a third, separate, class. The location of these 2 neurons was on the border of L3–L5 and these 2 neurons were later actually classified as L5 neurons in the CA that included all pyramidal neurons (Fig. 5*A*,*E* and Supplementary Fig. 6*C*). Although the field span of the apical dendrite showed similar measures for a subset of slender and broad pyramidal neurons, broad tufted neurons usually displayed a more dense apical tree with more branches and a higher total length of the apical dendrite (Fig. 2*B* and Supplementary Table 4). All RS neurons had broad apical tufts, whereas all bursting L3 neurons had slender tufts. Adapting neurons had either broad or slender morphologies (Supplementary Table 3).

Because the CA of morphological and electrophysiological parameters led to very similar categorizations (Supplementary Tables 3 and 4), we combined morphological and electrophysiological parameters in one CA (Fig. 2*C*). This resulted in 3 main subclasses: broad tufted RS neurons (RS, $n = 6$, or 29%), broad tufted adapting neurons ($n = 4$, or 19%), and slender tufted neurons ($n = 11$, or 52%; Fig. 2*C*–*F* and Table 5). The slender tufted neurons could be subdivided further in those with an adapting ($n = 5$, or 24%) and those with a bursting firing pattern ($n = 6$, or 29%). The total length and the number of apical dendritic collaterals of slender tufted neurons was about half that of broad tufted L3 pyramidal neurons. However, the properties of the basal dendrites of these L3 pyramidal subtypes did not differ (Table 5). Electrophysiologically, slender tufted neurons had a more depolarized RMP of −66.6 ± 0.6 mV and a larger voltage sag ($n = 11$; Table 5); in contrast, both broad tufted RS and broad tufted adapting L3 pyramidal neurons showed little if any voltage sag and had RMPs of −78.8 ± 0.8 and −71.5 ± 1.9 mV, respectively ($P < 0.001$ between all groups). Slender tufted bursting neurons and slender tufted adapting neurons were very similar, and differed only in the slope of the firing rate (Fig. 2*E*,*F*). Their similar morphology and values for other electrophysiological properties explain why these subtypes are clustered together in the CA. However, because bursting neurons were very distinct in their firing rate, we considered these neurons as a separate subtype.

To summarize, based on morphological and electrophysiological parameters 4 pyramidal cell subtypes could be characterized in L3: broad tufted RS neurons, broad tufted adapting neurons, slender tufted adapting neurons, and slender tufted bursting neurons. The last subtype is unique for L3 and was not observed in any of the other layers of the mPFC.

Layer 5 Pyramidal Neurons

Pyramidal neurons in L5 are the best studied cell type in the mPFC, and they have been categorized according to their electrophysiological and morphological properties (Yang et al. 1996; Degenetais et al. 2002; Wang et al. 2006; Chang and Luebke 2007). However, an unsupervised CA combining morphological and physiological properties has not been performed to date. Previous studies have used the membrane R_{in}, the AP firing pattern (RS, adapting or burst firing), and the AP waveform (presence of a depolarizing after potential (DAP)) (Yang et al. 1996; Degenetais et al. 2002; Chang and Luebke 2007) to categorize these neurons. Morphologically, L5 pyramidal cells can be categorized as "broad tufted" L5 pyramidal neurons that possess a complex apical dendrite with numerous

Table 4

Electrophysiological subtypes of L2 pyramidal neurons differ in adaptation ratios, but not in passive electrical properties or morphological parameters

	Regular spiking ($n = 3$)	Ad-RS ($n = 4$)	Adapting ($n = 8$)	P
Electrophysiology				
Ratio ISI-1/ISI-9	**0.32 ± 0.05***	0.19 ± 0.02	0.15 ± 0.02	**<0.05**
Ratio ISI-2/ISI-9	0.71 ± 0.03	0.49 ± 0.07	0.34 ± 0.05	**<0.01**
Ratio ISI-3/ISI-9	0.86 ± 0.02	0.82 ± 0.02	**0.50 ± 0.06****	**<0.01**
Increase in firing frequency (Hz/100 pA)	8.1 ± 1.1	5.3 ± 0.4	5.1 ± 0.4	**<0.05**
Membrane potential (mV)	−78.5 ± 2.5	−74.3 ± 1.0	−77.3 ± 2.8	0.38
Input resistance (MΩ)	218 ± 65	149 ± 10	162 ± 17	0.15
Rheobase (pA)	183 ± 43	183 ± 14	203 ± 26	0.79
Time constant (ms)	17.3 ± 1.2	19.6 ± 1.5	21.8 ± 2.4	0.18
Voltage sag (%)	1.5 ± 0.8	2.8 ± 0.7	3.7 ± 2.0	0.34
Morphology				
Location in L2 (%)	57 ± 9	75 ± 10	71 ± 11	0.50
Field span apical dendrites (μm)	290 ± 43	324 ± 29	376 ± 25	0.22
Field span basal dendrites (μm)	203 ± 9	178 ± 18	213 ± 9	0.21
Total length apical dendrites (μm)	3066 ± 341	3621 ± 397	3669 ± 521	0.62
Total length basal dendrites (μm)	1530 ± 230	1452 ± 259	2090 ± 239	0.19
Soma (μm^2)	216 ± 7	196 ± 16	218 ± 9	0.39
Number of apical branches	28.0 ± 2.1	29.0 ± 4.7	29.5 ± 3.3	0.96
Number of basal branches	17.0 ± 1.5	17.8 ± 1.6	25.5 ± 4.0	0.12

Note: For clarity, the results of the post hoc comparison of groups is only given (values in bold followed with asterisks) when a cell type is different from all other cell types. *$P < 0.05$, **$P < 0.01$.

branches, or "slender tufted" L5 pyramidal neurons that have a more restricted field span of the apical dendritic tree and less side branches (Wang et al. 2006).

To characterize L5 pyramidal subtypes using unsupervised CA, we recorded 65 L5 pyramidal neurons, of which 62 neurons could be morphologically reconstructed (see Supplementary Fig. 4 for reconstructions of L5 neurons). For 4 morphological identified neurons, we did not obtain electrophysiological data.

The majority of L5 pyramidal neurons showed clear apical dendrites with bifurcations in L1, that could be characterized either as slender or broad tufts (Fig. 3*B*). Only a few L5 neurons were untufted ($n = 3$ of 62, 5%; Supplementary Fig. 4). In one instance, a L5 pyramidal neuron with a secondary main dendrite was observed (Supplementary Fig. 4). Electrophysiologically, L5 pyramidal neurons displayed RS or adapting firing trains (Fig. 3*A*). A minority of neurons responded with an AP doublet upon current stimulation (5 of 61; ~8%). Increasing the stimulation strength always revealed an adapting firing pattern of these neurons, which was indistinguishable from that of other adapting neurons; bursts of APs as seen in some L3 pyramidal neurons were never observed under our recording conditions. Notably, the first interspike interval became considerably shorter for all L5 pyramidal neurons with higher stimulation strength, as was also the case for L2 and L3 pyramidal neurons.

A CA based on morphological or electrophysiological parameters alone resulted in 3 main groups of L5 neurons, with considerable overlap (Table 1 and Supplementary Tables 5 and 6). A CA with combined morphological and electrophysiological parameters was performed. L5 pyramidal neurons could be categorized as broad tufted RS neurons exhibiting a wide and complex apical dendritic tree ($n = 18$ or 31%) and slender tufted, adapting neurons with simpler and fewer apical oblique and tuft dendrites ($n = 40$ or 69%, Fig. 3*A–C*). Slender tufted adapting L5 pyramidal neurons could be further subdivided into those with a high cellular input resistance (Ad-HR, $n = 13$, or 22%) and those with a lower input resistance (Ad-LR, $n = 27$, or 47%, $P < 0.001$ between all subtypes, Table 6). In addition, the 2 slender-adapting subtypes differed in their basal dendritic morphology: Ad-HR neurons had a reduced total dendritic length and a lower number of basal branches compared with Ad-LR and RS pyramidal neurons ($P < 0.001$, Table 6). Thus, in contrast to L3 pyramidal neurons, the morphology of the basal dendritic arbor is a relevant parameter for the definition of L5 pyramidal subtypes.

In general, L5 pyramidal neurons had larger cell bodies than pyramidal neurons in other layers (Table 2 and Supplementary Fig. 1). Among the different L5 subtypes, broad tufted neurons had the largest soma size (Table 6). The relative location of L5 subtypes within L5 was not different and all cell classes could be found in either superficial or deep L5 (Table 6 and Supplementary Fig. 4).

Electrophysiologically, L5 pyramidal subtypes differed substantially in their excitability. RS neurons were the least excitable with an average rheobase value of 179 ± 10 pA, followed by Ad-LR neurons with 124 ± 7 pA. Ad-HR neurons could be brought to spike with only 66 ± 4 pA, a value that is almost threefold lower than that for RS neurons ($P < 0.001$ between all subtypes, Table 6).

The size of the voltage sag was among the most variable parameters with a coefficient of variation of 0.43. Virtually, all L5 pyramidal neurons displayed a voltage sag, suggesting that HCN channels are expressed in L5 pyramidal subtypes, albeit to a different extent. We calculated the percentage voltage sag in response to a negative current step that caused an approximately −7.5 mV hyperpolarization of the membrane potential (see Materials and Methods). In this way, differences in input resistances are compensated for. Large voltage sags (>13% sag) were present in broad tufted RS L5 neurons, whereas both types off adapting L5 neurons could display large or small voltage sags (<13% sag, Fig. 3*F* and Table 6, large voltage sags: 18 of 18 (100%) RS neurons, 6 of 13 (46%) Ad-HR neurons, 5 of 27 (56%) Ad-LR neurons, $P < 0.01$).

Another parameter used to classify L5 pyramidal neurons is the presence of a DAP (Fig. 3*G*) (Yang et al. 1996). DAPs were common among RS neurons but more rare among adapting neurons (DAP present: 76% (RS), 38% (Ad-HR), and 22% (Ad-LR), χ^2 test $P < 0.01$).

To summarize, pyramidal neurons in L5 can be subdivided in 3 subtypes: 1) Broad tufted RS neurons, 2) slender tufted

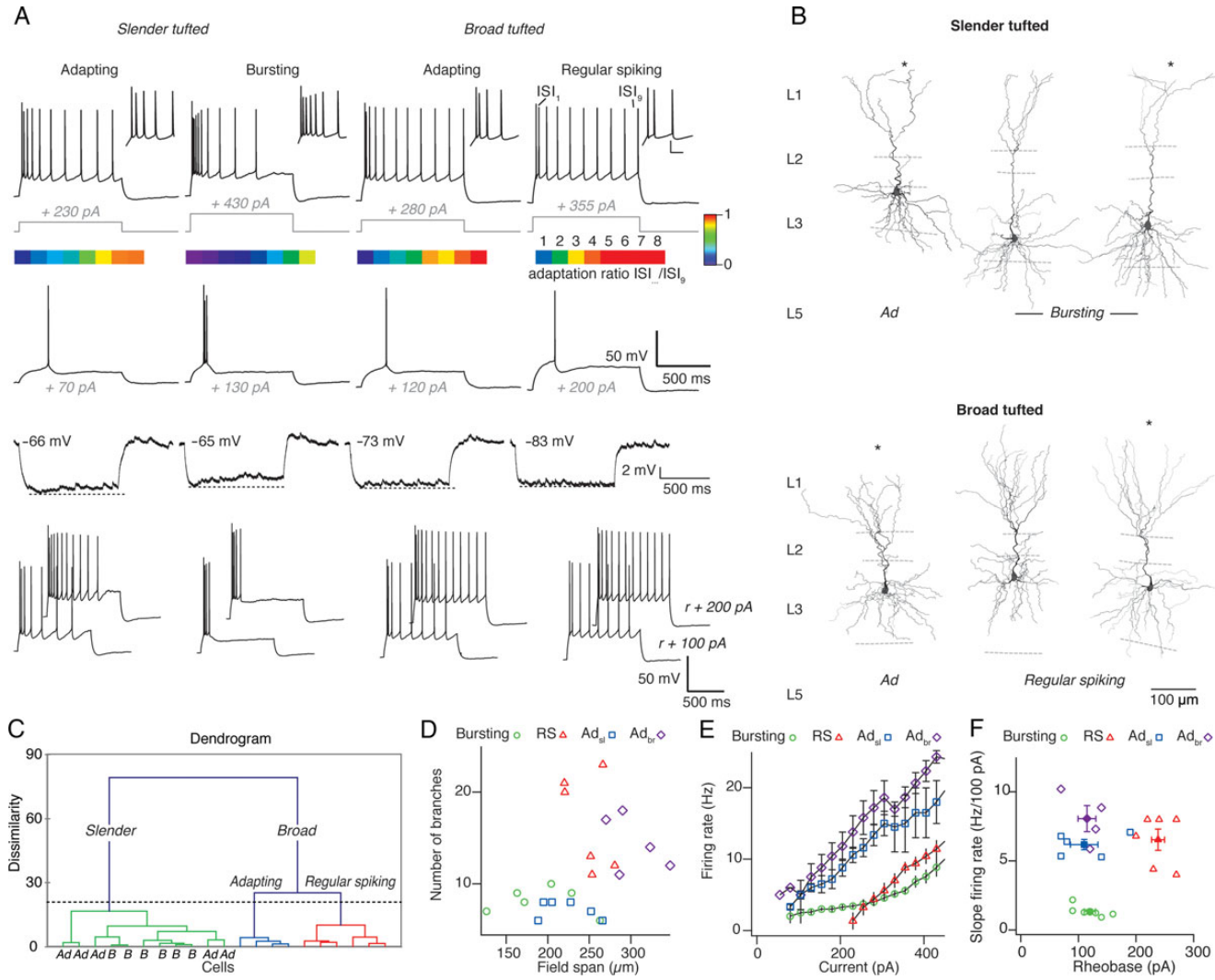

Figure 2. Pyramidal neuron subclasses in layer 3. (*A*) Electrophysiological profile of L3 subtypes: slender tufted adapting or bursting neurons (left), and broad tufted adapting or regular spiking neurons (right). Top, voltage response when a minimum of 10 action potentials were elicited with corresponding current steps in gray. The inset shows a magnification of the first spikes (scale bar: 25 mV, 50 ms). Beneath, adaptation ratios from interspike interval 1–8 with the 9th interspike interval (ISI-9) as shown in color code. Middle, response to the first current step that initiated an action potential (rheobase value), and to a hyperpolarizing current injection that would hyperpolarize the neurons with ~7.5 mV. Bottom, responses to the rheobase value + 100–200 pA reveal a low increase in action potential number for bursting neurons upon increased current stimulation. Note that bursting neurons often show a doublet or triplet at rheobase values. (*B*) Morphological reconstruction of dendrites from L3 pyramidal cells. Top, example neurons with slender tufted apical dendrites, bottom example neurons with broad tufted apical dendrites. Note that slender tufted neurons show less bifurcations and branches of apical dendrites. Below each neuron the electrophysiological subtype is indicated. (*C*) Dendrogram resulting from CA of electrophysiological and morphological parameters reveals 3 main clusters. Dashed line indicates the threshold as determined by the Thorndike procedure. Slender tufted neurons included both adapting (Ad) and bursting (B) neurons. (*D*) L3 subtypes differ in field span and/or number of branches of the apical dendrite. Note that all bursting neurons were slender tufted, whereas all RS neurons were broad tufted. Adapting neurons could have slender or broad tufted morphologies. (*E*) Firing rate as a function of injected current. Note that this relation is nonlinear for bursting pyramidal neurons. (*F*) Initial slope of firing rate as a function of current plotted against rheobase. Averages for regular spiking (triangles), bursting (circles), slender tufted adapting (squares), and broad tufted adapting (diamonds) neurons are shown with error bars.

adapting neurons with a high R_{in}, and (3) Slender tufted adapting neurons with low R_{in}. The latter 2 subclasses also differ in other physiological and morphological properties. Large voltage sags and the presence of a DAP were more common in RS neurons, but not exclusively so. The 3 subtypes were present throughout L5, without any preference for either superficial or deep L5.

Layer 6 Pyramidal Neurons

We recorded and reconstructed 18 L6 pyramidal neurons, of which 14 neurons were selected for electrophysiological data analysis (see Supplementary Fig. 5 for reconstructions of L6 neurons).

We found that L6 pyramidal neurons in the mPFC showed a great morphological variety (Fig. 4*A* and Supplementary Fig. 5), ranging from neurons with apical dendrites that spanned all cortical layers and terminated in L1 to small L6 pyramidal neurons with a dendritic tree that was exclusively restricted to L6. Also, the horizontal field span of L6 pyramidal neurons was very diverse: Pyramidal neurons with both the broadest and the smallest field span of all mPFC pyramidal neurons were found in L6. Some L6 pyramidal neurons had inverted apical dendrites pointing towards the white matter. The high

Table 5
L3 pyramidal neuron subtypes differ in electrophysiological and morphological parameters

	Slender tufted		Broad tufted		*P*
	Adapting ($n = 5$)	Bursting ($n = 6$)	Adapting ($n = 4$)	Regular spiking ($n = 6$)	
Electrophysiology					
Ratio ISI-1/ISI-9	0.15 ± 0.03	0.09 ± 0.02	0.11 ± 0.01	0.21 ± 0.05	0.07
Ratio ISI-2/ISI-9	0.28 ± 0.06	0.14 ± 0.04	0.28 ± 0.03	0.51 ± 0.10	**<0.01**
Ratio ISI-3/ISI-9	0.42 ± 0.07	0.21 ± 0.06	0.53 ± 0.04	0.77 ± 0.08	**<0.01**
Increase in firing frequency (Hz/100 pA)	6.1 ± 0.3	**1.3 ± 0.2****	8.0 ± 1.0	6.5 ± 0.8	**<0.01**
Membrane potential (mV)	−67.0 ± 0.1	−66.2 ± 1.0	−71.5 ± 1.9	**−78.8 ± 0.8****	**<0.01**
Input resistance (MΩ)	152 ± 24	138 ± 13	185 ± 9	143 ± 10	0.21
Rheobase (pA)	110 ± 24	122 ± 11	115 ± 16	**238 ± 11****	**<0.01**
Time constant (ms)	32.0 ± 5.9	27.6 ± 1.3	27.1 ± 2.7	18.7 ± 0.5	**0.04***
Voltage sag (%)	11.7 ± 3.2	11.7 ± 1.5	3.0 ± 1.4	0.2 ± 0.4	**<0.01**
Morphology					
Location in L3 (%)	62 ± 14	49 ± 8	29 ± 6	21 ± 7	**0.02***
Field span apical dendrites (μm)	214 ± 12	193 ± 20	312 ± 14	249 ± 10	**<0.01**
Field span basal dendrites (μm)	338 ± 56	276 ± 13	270 ± 19	252 ± 17	0.23
Total length apical dendrites (μm)	1081 ± 89	1244 ± 119	2011 ± 146	2448 ± 265	**<0.01**
Total length basal dendrites (μm)	3733 ± 734	3123 ± 248	2609 ± 330	2901 ± 243	0.36
Soma (μm^2)	258 ± 32	193 ± 20	178 ± 14	181 ± 7	**0.05***
Number of apical branches	7.4 ± 0.4	7.5 ± 0.6	13.8 ± 1.5	16.7 ± 2.1	**<0.01**
Number of basal branches	26.2 ± 3.0	24.0 ± 2.5	23.5 ± 3.2	25.3 ± 1.3	0.87

Note: For clarity, the results of the post hoc comparison of groups is only given (values in bold followed with asterisks) when a cell type is different from all other cell types. *$P < 0.05$, **$P < 0.01$.

percentage of L6 pyramidal neurons with apical dendrites ascending to L1 appears to be a characteristic feature of L6 pyramidal neurons in the mPFC: In our study, 39% of L6 neurons exhibited such long apical dendrites, whereas a fraction of <5% has been reported in other cortical areas (Katz 1987; Van Brederode and Snyder 1992; Bailey et al. 2012).

L6 pyramidal neurons appeared to be less diverse with respect to their electrophysiological properties. Although L6 neurons show variations in active and passive properties, this was perhaps less than one could expect given the substantial morphological diversity between these neurons. For example, 11 of 14 L6 pyramidal neurons displayed a RS firing pattern (Fig. 4*B*,*C* and Table 7). The 3 exceptions were neurons, one of which had an accelerating firing pattern, an adapting firing pattern, and a firing pattern with an initial burst of 3 AP followed after a longer ISI by RS. Of note is that the RS neurons in L6 showed a more RS right from the beginning of the voltage step; they lacked the very short first ISI seen in RS neurons from other layers ($P < 0.01$ compared with other layers, Fig. 4*B* and Table 3). Another property that set L6 pyramidal neurons apart from pyramidal neurons in other layers was the steep increase of the firing frequency upon increased current injection (Table 3), a feature that can be explained by the high cellular R_{in} of these neurons. Note however that adapting L5 pyramidal neurons with a similarly high cellular R_{in} (L5 Ad-HR neurons) had input–output relationships with much shallower slopes (input resistance: 255 ± 20 MΩ (L5 Ad-HR), 306 ± 30 MΩ (L6), $P = 0.17$; slope 6.4 ± 0.7 Hz/100 pA (L5 Ad-HR), 15.0 ± 1.5 Hz/100 pA (L6), $P < 0.001$).

Because almost all L6 pyramidal neurons showed a RS firing pattern, we performed a CA based on passive physiological properties alone (Table 1); however, the resulting clusters did not differ in their morphological properties (Supplementary Table 7). Similarly, a CA based only on morphological properties did not reveal any clear differences in the physiological parameters (Table 7). Therefore, it appears that for L6 pyramidal neurons, like L2 pyramidal neurons, there is no clear correlation between the electrophysiological properties and the dendritic morphology. The CA based on the morphological properties of L6 pyramidal neurons alone revealed 3 main clusters: 1) tall L6 pyramidal neurons with apical dendrites projecting to L1 ($n = 5$ or 28%); 2) wide L6 pyramidal neurons with very large field spans of basal dendrites ($n = 3$ or 18%); 3) short L6 pyramidal neurons with apical dendrites confined to L3–L6 ($n = 10$ or 56%, Table 7). This last category could be subdivided in short L6 pyramidal neurons with a wider field span of basal dendrites ("short and broad", $n = 5$ or 28%) and L6 pyramidal neurons with more confined dendritic trees ("small", $n = 5$ or 28%). Short and broad L6 neurons had simpler and fewer apical oblique and tuft dendrites compared with tall L6 neurons (Table 7 and Supplementary Fig. 5).

To summarize, L6 pyramidal neurons are more diverse in their morphological appearance than pyramidal neurons in other layers. L6 pyramidal neurons in the mPFC often have apical dendrites that extend to L1. Physiologically, L6 neurons displayed RS firing patterns, had a high cellular R_{in} and were highly excitable in comparison to pyramidal neurons from other layers (Tables 2 and 3).

CA of Pyramidal Neurons of all Layers

Finally, we performed a CA on the pyramidal neurons from all layers. We included all morphological and electrophysiological parameters listed in Table 8. This enabled us to compare how different the pyramidal subtypes are in comparison to each other. The CA revealed 4 main subtypes: 1) RS L5 neurons constituted the first cluster; 2) adapting L5, adapting L3 and bursting L3 neurons constituted the second cluster; the third 3) cluster contained all L2 pyramidal neurons and RS L3 neurons; and lastly, the fourth (4) cluster consisted of L6 pyramidal neurons. Further subdivision of the second cluster at a lower cutoff led to a separation of adapting L5 neurons with high or low cellular input resistances (L5-HR and L5-LR) and L3 bursting and broad tufted adapting pyramidal neurons, further subdivision of the third cluster led to a separation of L2 and RS L3 neurons, and further subdivision of the fourth cluster led to a separation of tall and small L6 neurons (Fig. 5*A*).

The results from this CA show that RS L5 neurons are the most distinct pyramidal neuron subtype in the mPFC. These

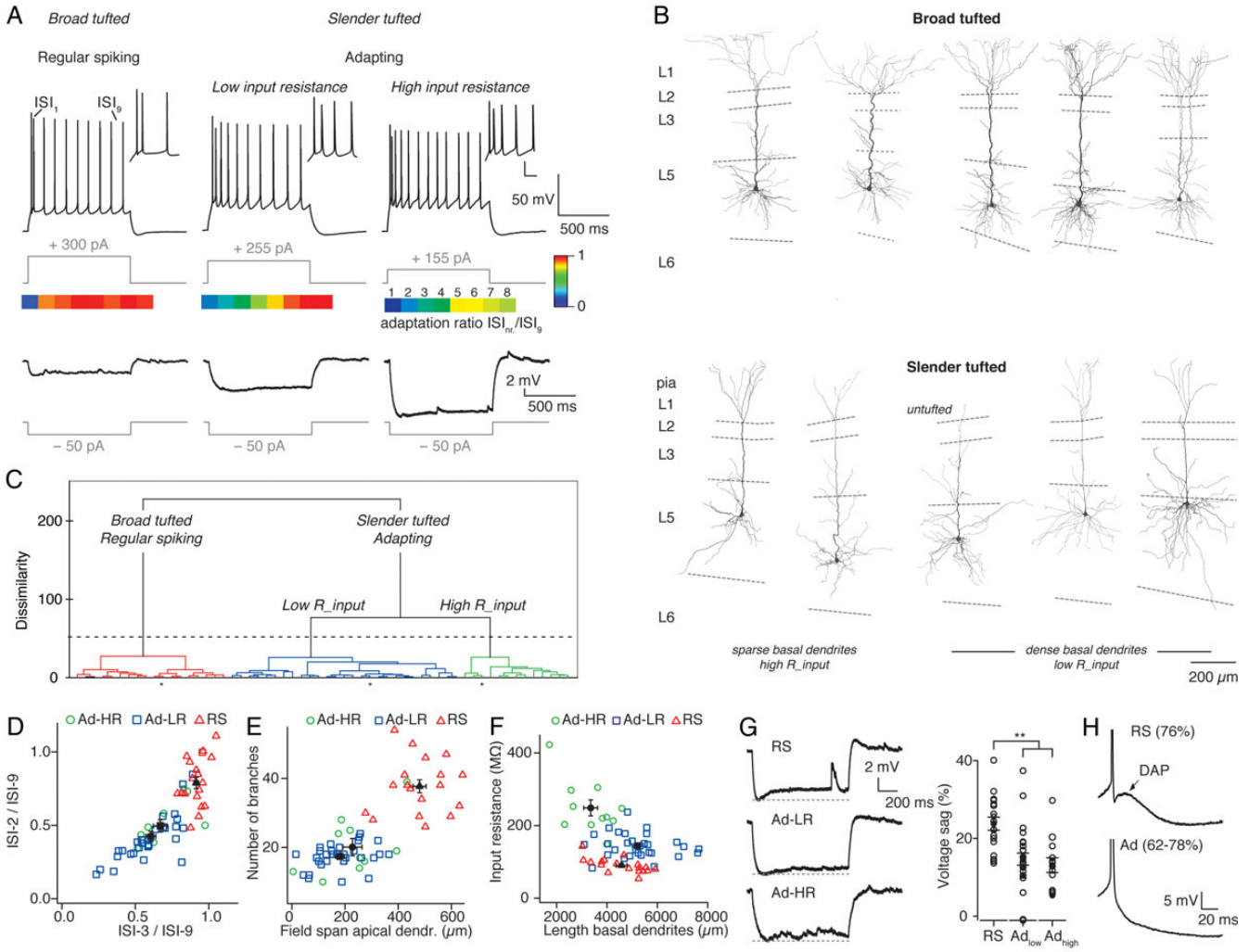

Figure 3. Pyramidal neuron subclasses in layer 5. (*A*) Electrophysiological profile of L5 neurons. The upper panel shows the response when a minimum of 10 action potentials were elicited with corresponding current steps in gray. The inset shows a magnification of the first 3–4 spikes (scale bar: 25 mV, 50 ms). Beneath, adaptation ratios from interspike interval 1–8 with the 9th interspike interval (ISI9) are shown in color code. The lower panel shows the response (black) to a hyperpolarizing step of –50 pA (gray). Note the different size of the voltage response due to different values for the cellular input resistance. (*B*) Morphological reconstruction of dendrites from L5 pyramidal neurons. Top, example neurons with broad tufted apical dendrites. Bottom, example neurons with slender tufted apical dendrites. Below each neuron morphological and/or electrophysiological subclasses are indicated. Note the examples of rare subtypes like pyramidal neurons with a double apical dendrite (top right) or an untufted apical dendrite (bottom, middle). (*C*) Dendrogram resulting from CA of electrophysiological and morphological parameters (Table 1) reveals 3 main clusters. Asterisks mark the example neurons shown in A. (*D*) Regular spiking (RS) neurons have higher adaptation ratios than adapting neurons with low (Ad-LR) or high (Ad-HR) input resistance ($P < 0.01$). (*E*) The dendritic tree of the apical dendrite of RS neurons has a wider field span and more branches than the apical dendrite of Ad-LR and Ad-HR neurons ($P < 0.01$). (*F*) Ad-HR neurons have sparser basal dendrites and a higher cellular input resistance compared with RS and Ad-LR neurons ($P < 0.01$). RS and Ad-LR neurons differed in cellular input resistance ($P < 0.01$), but not in the total length of the basal dendrites. (*G*) RS neurons have on average a larger voltage sag compared with Ad-LR or Ad-HR neurons ($P < 0.01$). Left, example traces: the sag is calculated as the percentage change from the maximal response to hyperpolarizing step of ~ –7.5 mV. Also note the difference in the membrane time constant for the 3 subtypes. (*H*) RS neurons had more often depolarizing after potentials (DAPs) than Ad-HR or Ad-LR neurons ($P < 0.01$).

neurons had the longest dendritic length, the highest number of apical oblique and tuft branches and the largest cell somata of all subtypes ($P < 0.01$, Tables 3–6). In addition, RS L5 neurons had the most pronounced voltage sags ($P < 0.01$, Tables 3–6).

The CA also indicates that bursting and adapting L3 neurons resemble more adapting L5 neurons, while RS L3 neurons are more similar to L2 neurons. Indeed, physiological properties in which RS L3 pyramidal neurons are distinct from other L3 neurons were similar to the characteristics of L2 neurons such as a high rheobase value and a slow membrane time constant (Table 3). However, morphologically, L2 and L3 neurons differ in the ratio of apical and basal field span and relative total length of apical and basal dendrites ($P < 0.01$, Table 2). L3 bursting neurons and broad tufted adapting L3 neurons still existed as subgroups in the CA, stressing the unique characteristics of these subtypes. Slender tufted adapting L3 pyramidal neurons were more similar to slender tufted adapting L5 neurons and mixed with this subgroup.

Apart from slender tufted L3 neurons, practically all other individual neurons followed the laminar subdivision of cell types (94 from 103 neurons). Notably, leaving out the parameter of the cortical location would lead to the exact same classification for 99 from 103 neurons, underscoring the point that laminar subtypes have truly unique characteristics. For example, leaving out the cortical location of neurons did not group RS L5 pyramidal neurons together with RS L3

Table 6
L5 pyramidal neuron subtypes differ in electrophysiological and morphological parameters

	Slender tufted		Broad tufted	
	High-resistance ($n = 13$)	Low-resistance ($n = 27$)	Regular spiking ($n = 18$)	P
Electrophysiology				
Ratio ISI-1/ISI-9	0.25 ± 0.03	0.22 ± 0.01	0.22 ± 0.02	0.70
Ratio ISI-2/ISI-9	0.43 ± 0.05	0.46 ± 0.03	**0.79 ± 0.04****	**<0.01**
Ratio ISI-3/ISI-9	0.56 ± 0.06	0.65 ± 0.03	**0.91 ± 0.02****	**<0.01**
Increase in firing frequency (Hz/100 pA)	6.4 ± 0.7	5.6 ± 0.4	6.4 ± 0.2	0.27
Membrane potential (mV)	−65.5 ± 0.09	−67.4 ± 0.6	−64.0 ± 0.7	**<0.01**
Input resistance (MΩ)	**255 ± 20****	**145 ± 6****	**90 ± 5****	**<0.01**
Rheobase (pA)	**66 ± 4****	**124 ± 7****	**179 ± 10****	**<0.01**
Time constant (ms)	**40.1 ± 2.4****	**31.9 ± 1.3****	**21.2 ± 1.0****	**<0.01**
Voltage sag (%)	13.1 ± 1.9	14.7 ± 1.5	**23.8 ± 1.7****	**<0.01**
Morphology				
Location in L5 (%)	34 ± 6	30 ± 4	38 ± 4	0.50
Field span apical dendrites (μm)	307 ± 31	288 ± 19	**482 ± 24****	**<0.01**
Field span basal dendrites (μm)	403 ± 60	394 ± 10	325 ± 9	0.07
Total length apical dendrites (μm)	3346 ± 462	3187 ± 113	**6530 ± 310****	**<0.01**
Total length basal dendrites (μm)	**3271 ± 219****	5260 ± 224	4580 ± 220	**<0.01**
Soma (μm^2)	301 ± 18	298 ± 11	**367 ± 19****	**<0.01**
Number of apical branches	19.2 ± 2.2	17.7 ± 0.7	**37.7 ± 1.9****	**<0.01**
Number of basal branches	**21.3 ± 1.7****	**31.0 ± 1.2***	**36.8 ± 1.7****	**<0.01**

Note: For clarity, the results of the post hoc comparison of groups is only given (values in bold followed with asterisks) when a cell type is different from all other cell types. *$P < 0.05$, **$P < 0.01$.

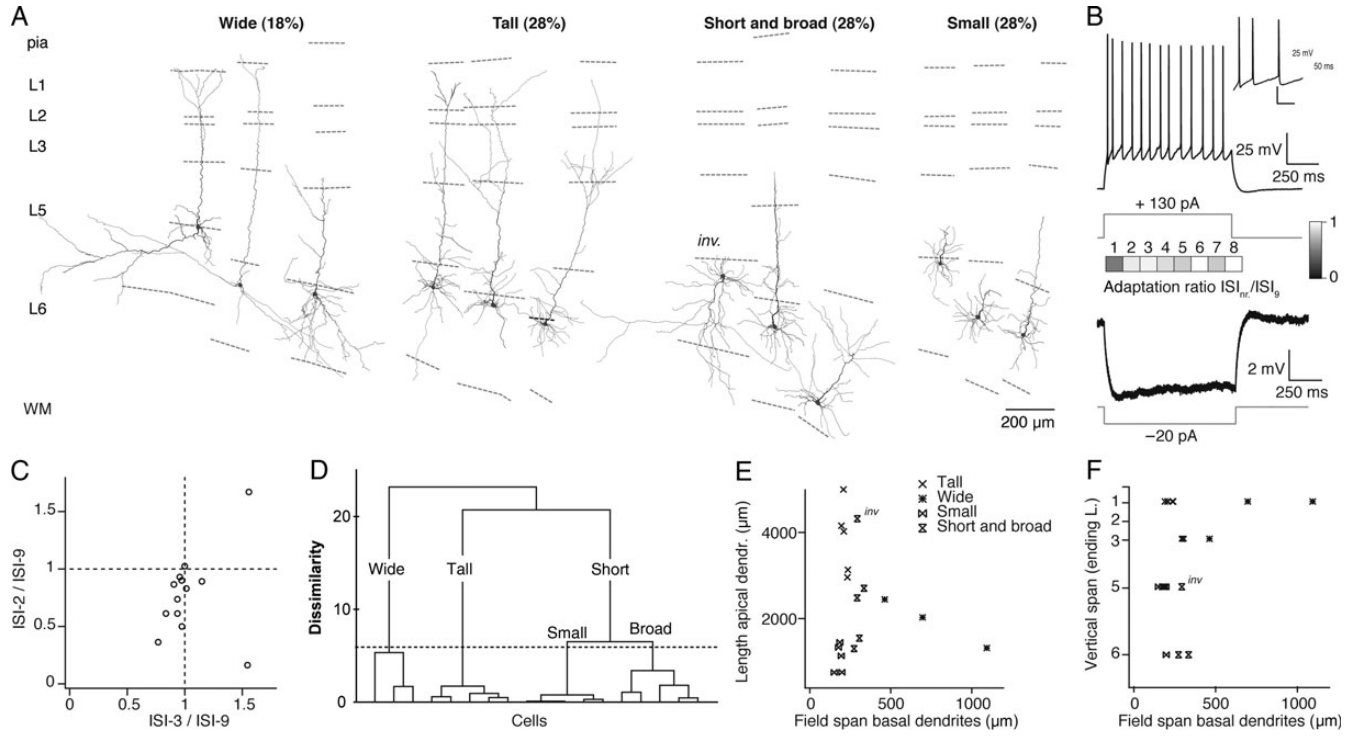

Figure 4. Layer 6 pyramidal neurons. (*A*) Morphological reconstruction of soma and dendrites from L6 pyramidal neurons. Note the large diversity in horizontal and vertical span of dendrites. (*B*) Electrophysiological profile of a typical regular spiking L6 neuron: the upper panel shows the response when a minimum of 10 action potentials were elicited with the corresponding current step in gray. Beneath, adaptation ratios from interspike interval 1–8 with the 9th interspike interval (ISI9) are shown in color code. Note that the ratio of ISI1/ISI9 is higher compared with pyramidal neurons in other layers. The lower panel shows the response to a hyperpolarizing step of −20 pA. Note that this small current injection already causes a large hyperpolarization due to the high cellular input resistance of L6 neurons. (*C*) The majority of L6 neurons showed a regular spiking firing pattern. (*D*) Dendrogram from CA of morphological parameters. (*E*) L6 pyramidal subtypes differ in length of apical dendrites and the field span of basal dendrites. (*F*) L6 pyramidal subtypes differ in their vertical span, expressed as the layer where the apical dendrite terminates or "ending layer." Note that the short neuron with a high apical dendritic length had an inverted apical dendrite (inv).

pyramidal neurons. Apart from morphological differences between RS neurons from different layers, these neurons also differ in their passive physiological properties (Supplementary Table 8). Similarly, adapting neurons from different layers differed in almost every physiological parameter (Supplementary Table 9).

For 9 of 103 neurons, the CA of all neurons suggested a different layer for their soma location than that we had

Table 7
Morphological subtypes in L6 differ only marginally in electrophysiological properties

	Tall L6	Wide L6	Short L6	Small L6	*P*
Morphology	$N = 5$	$N = 3$	$N = 5$	$N = 5$	
Location in L6 (%)	31% ± 6%	13% ± 8%	49% ± 17%	30% ± 9%	0.28
Field span apical dendrites (μm)	295 ± 27	201 ± 63	361 ± 127	147 ± 10	0.22
Field span basal dendrites (μm)	215 ± 8	**751 ± 184****	300 ± 10	181 ± 8	**<0.01**
Total length apical dendrites (μm)	**3853 ± 371***	1930 ± 329	2470 ± 533	1083 ± 144	**<0.01**
Total length basal dendrites (μm)	1685 ± 250	**3387 ± 487***	**2464 ± 187***	1597 ± 131	**<0.01**
Soma (μm^2)	186 ± 20	189 ± 24	218 ± 24	185 ± 9	0.57
Number of apical branches	**25.2 ± 2.5***	9.0 ± 3.6	15.0 ± 4.5	13.6 ± 2.1	**0.03***
Number of basal branches	19.6 ± 2.8	17.3 ± 3.8	21.2 ± 3.6	18.0 ± 3.1	0.85
Vertical span (ending layer)	5 × L1	2 × L1 1 × L3	2 × L3 1 × L5 2 × L6	4 × L5 1 × L6	**<0.01**
Electrophysiology	$N = 4$	$N = 3$	$N = 4$	$N = 2$	
Ratio ISI-1/ISI-9	0.49 ± 0.05	0.35 ± 0.14	0.42 ± 0.12	1.06 ± 0.42	0.53
Ratio ISI-2/ISI-9	0.79 ± 0.07	0.58 ± 0.15	0.66 ± 0.19	1.28 ± 0.39	0.27
Ratio ISI-3/ISI-9	0.93 ± 0.03	0.88 ± 0.06	1.12 ± 0.14	1.35 ± 0.20	0.08
Increase in firing frequency (Hz/100 pA)	15.6 ± 1.5	12.2 ± 1.8	11.6 ± 1.8	24.8 ± 1.3	0.64
Membrane potential (mV)	−68.1 ± 1.9	−66.8 ± 0.8	−75.2 ± 2.9	−76.1 ± 1.3	**0.01***
Input resistance (MΩ)	276 ± 47	354 ± 85	236 ± 18	433 ± 40	0.67
Rheobase (pA)	78 ± 22	60 ± 10	125 ± 23	65 ± 5	0.32
Time constant (ms)	29.7 ± 4.0	33.1 ± 1.7	21.4 ± 4.7	21.8 ± 5.5	0.09
Voltage sag (%)	10.3 ± 2.5	13.1 ± 3.9	4.4 ± 2.9	6.9 ± 1.4	0.11

Note: For clarity, the results of the post hoc comparison of groups is only given (values in bold followed with asterisks) when a cell type is different from all other cell types. *$P < 0.05$, **$P < 0.01$. Note that, for vertical span, the χ^2 test was used. In the comparison of electrophysiological properties, "short" and "small" L6 pyramidal neurons were grouped to increase the number of observations. Short and small L6 pyramidal neurons are 2 subdivisions of the third cluster of the CA.

estimated ourselves (Fig. 5*B–E*). For 3 of those, the location of the soma was clearly within the layer as determined by us (Fig. 5*B* and Supplementary Fig. 6*A*,*B*). Thus, although these neurons showed more similarities with neurons in other layers than they were located in, we considered these neurons as rare exceptions. For 6 neurons, however, the location was not so clear-cut: these pyramidal neurons were all located at or near borders of mPFC layers (Fig. 5*C–E*). Because neuron types can intermingle around layer borders (Oberlaender et al. 2012), we decided to follow the CA for the final categorization for these 6 borderline cases. Although the number of neurons that had to be changed between the datasets for the individual layers was small, 6 of 103, we repeated the CA of the individual neurons to see how the addition and removal of these 6 neurons affected the clustering of the other neurons in each layer. Repeating the CA had no effect on the clustering of the remaining neurons in L2, L3, and L6. For L5 neurons, 2 from 58 neurons changed subclass after including more neurons to the CA. Thus, for the far majority of pyramidal neurons, the results from the CA of all neurons confirmed their membership of the subclass that was suggested by the CA of neurons within the individual layers. We found only 2 exceptions to this: first, the 3 "wide" pyramidal neurons that we first identified in L6, were all identified as L5 neurons in the CA of all neurons. The 2 neurons with the widest basal field span and the fewest arborizations (the left and middle neuron in Fig. 4*A*) appear to form a small subclass together with 2 L5 neurons (Fig. 5*A* and Supplementary Fig. 6*D–G*). Therefore, we have removed the wide subclass from L6 neurons in the overview that is given in Figure 6, and we consider these neurons as a rare subtype of L5 pyramidal neurons. Second, 4 from 5 slender tufted adapting neurons in L3 were categorized as slender tufted L5 neurons. Two of those were actually among the neurons that were located at the border, and thus may actually be L5 neurons. Nevertheless, the mixture of some of the remaining neurons shows that slender tufted adapting neurons from L3 are relatively similar to slender tufted adapting neurons from L5. This is specific for this L3 subclass only, as none of the bursting or broad tufted adapting L3 neurons were grouped together with L5 neurons.

Table 8
Parameters for CA of pyramidal neurons in L2–L6

Morphological
Location in cortex (%)
Field span tuft apical dendrites (μm)
Field span basal dendrites (μm)
Vertical span apical dendrites (ending layer)
Ratio field span apical/basal dendrites
Total length apical dendrites (μm)
Total length basal dendrites (μm)
Ratio length apical/basal dendrites
Sum length apical + basal dendrites (μm)
Soma (μm^2)
Number of apical branches
Number of basal branches
Total number of branches
Electrophysiological
Ratio ISI-1/ISI-9
Ratio ISI-2/ISI-9
Ratio ISI-3/ISI-9
Increase in firing frequency (Hz/100 pA)
Resting membrane potential (mV)
Input resistance (MΩ)
Rheobase (pA)
Time constant (ms)
Voltage sag (%)

Thus, a CA with physiological and morphological parameters grouped mPFC pyramidal neurons in 4 main clusters: 1) RS L5 neurons, 2) adapting and bursting L3 neurons and adapting L5 neurons, 3) L2 and RS L3 neurons, and 4) L6 neurons. Further subdivision revealed all subclasses that were identified from CAs of individual layers, except for slender tufted L3 adapting neurons. In addition, one new subclass emerged of wide pyramidal neurons that consisted of a L5 pyramidal neuron and pyramidal neurons that were located near the L5–L6 border. Importantly, repeating the CA without any parameter of cortical location lead to the same classification for

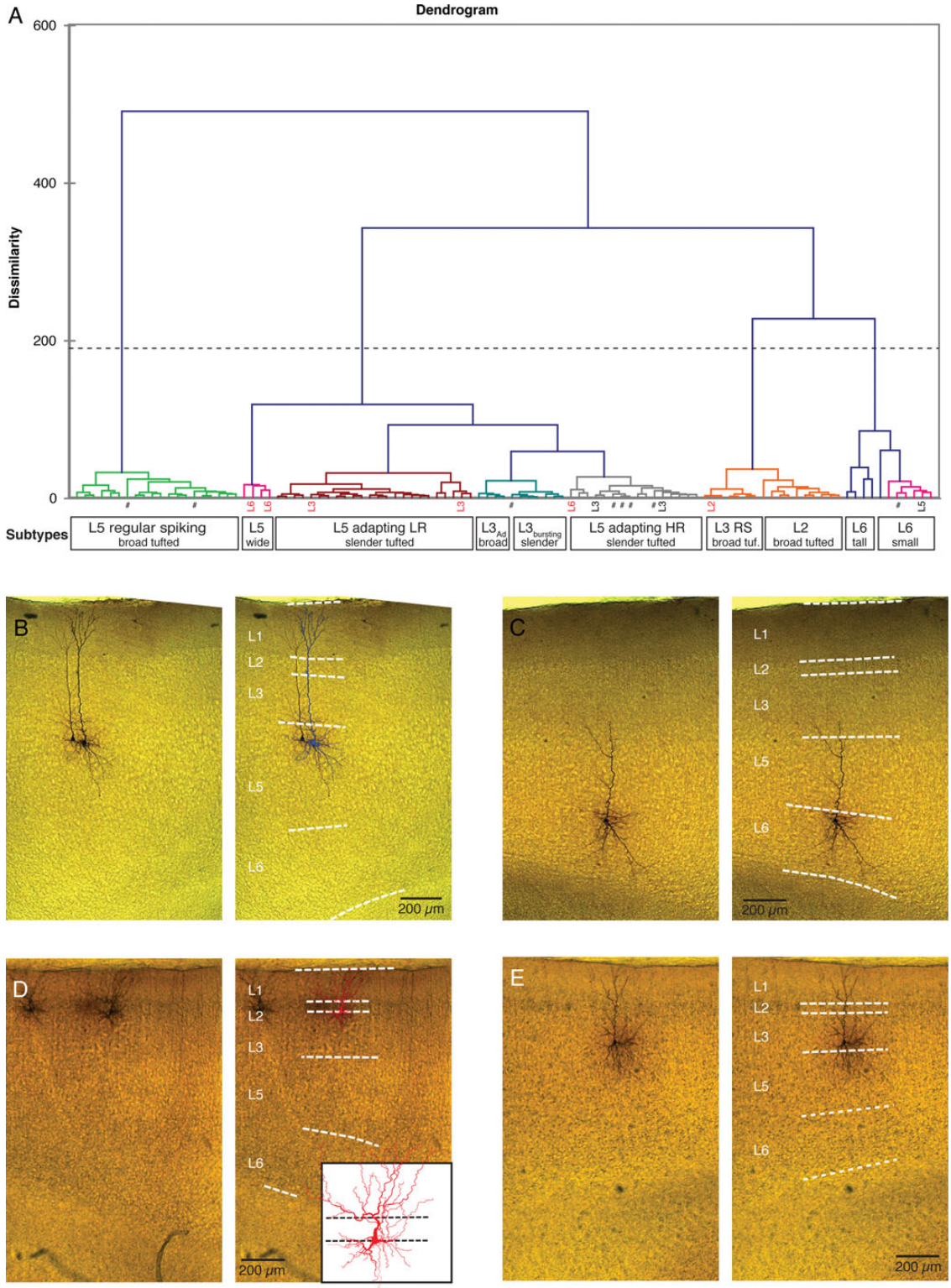

Figure 5. Pyramidal subtypes in the mPFC. (*A*) Dendrogram from CA of electrophysiological and morphological parameters (Table 8) reveals 4 main clusters and several subclusters. Neurons that are clustered in a subgroup from another cortical layer are indicated ("L…," $n = 9$). Six from these were located at layer borders (red colored "L…"). All L3 neurons that are marked are slender tufted adapting neurons ($n = 4$). Neurons that are clustered with another subtype of the same cortical layer are indicated with a cross (#, $n = 8$). For the remaining 86 neurons, the identity of the subtypes is as outlined at the bottom. (*B*) L5 neuron that was classified as L6 neuron is located at the upper part of L5. Layer borders are indicated at the right. Note that this L5 neuron resembled L6 neurons for several parameters such as total dendritic length, cellular input resistance and firing pattern. (*C*) L6 neuron that was classified as L5-HR neuron is located at the border of layers 5–6. Layer borders are indicated at the right. (*D*) L2 neuron that was classified as a L3-RS neuron is located at the border of layer 2–3. Layer borders are indicated at the right. Inset shows reconstructed neuron and borders of L2. (*E*) Slender tufted adapting L3 neuron that was classified as L5-LR neuron is located at the border of layer 3–5. Layer borders are indicated at the right.

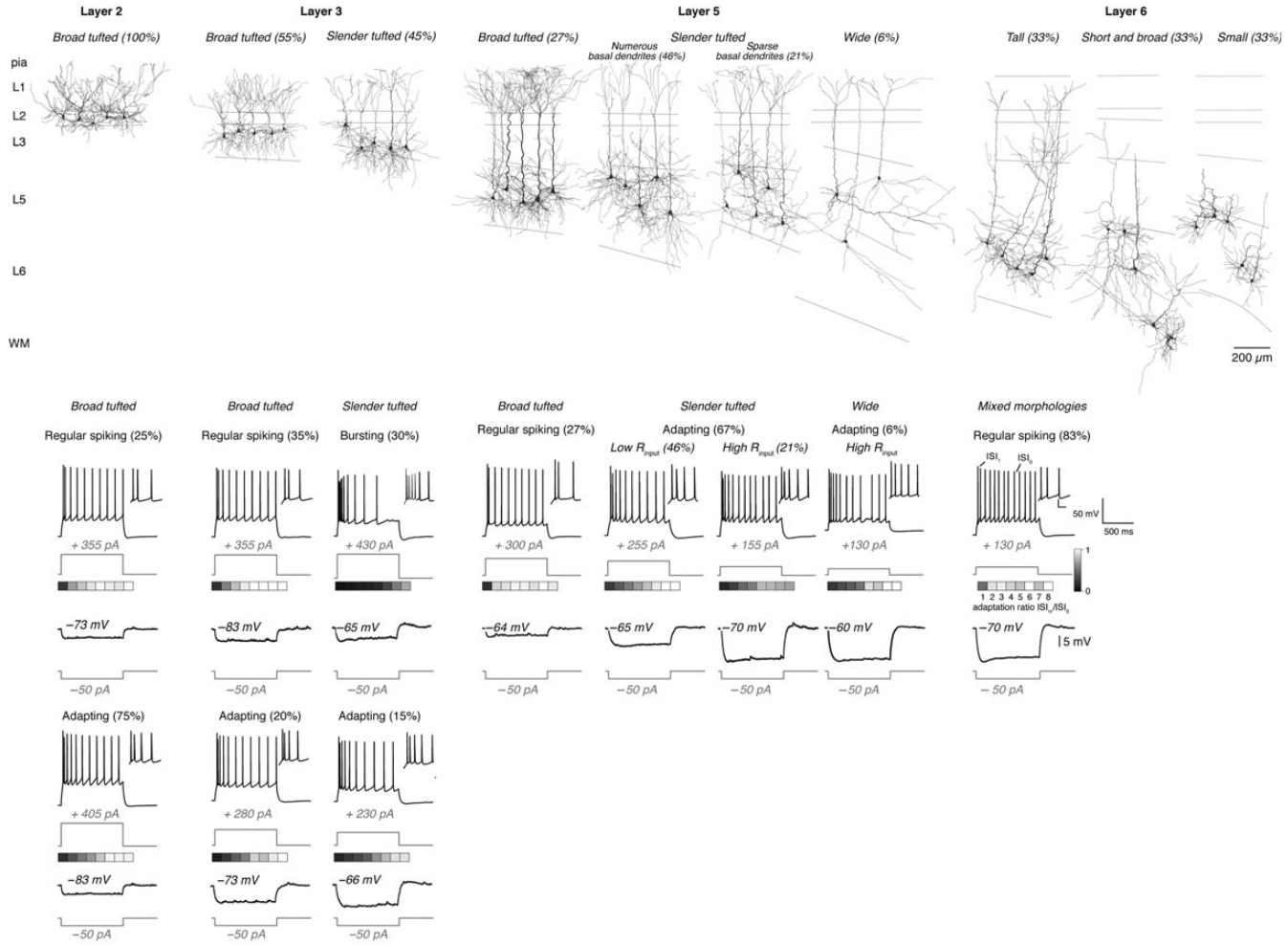

Figure 6. Overview of pyramidal subtypes in the rat mPFC. Top, morphological reconstruction of soma and dendrites of 5 example cells for each morphological subtype. Cortical layers are indicated with dashed lines. Bottom, electrophysiological profile of pyramidal subtypes: The upper panel shows the response when a minimum of 10 action potentials were elicited with corresponding current steps in gray. The inset shows a magnification of the first 3–4 spikes (scale bar: 25 mV, 50 ms). Beneath, adaptation ratios from interspike interval 1–8 with the 9th interspike interval (ISI-9) are shown in gray scale. The lower panel shows the response (black) to a hyperpolarizing step of −50 pA (gray). The resting membrane potential is indicated. Note the different size of the voltage response due to different values for the cellular input resistance.

99 from 103 neurons. These results underscore the point that subtypes have truly unique characteristics.

Discussion

We characterized pyramidal neurons throughout L2–L6 of the mPFC on the basis of their passive and active electrophysiological properties and their dendritic morphology (Fig. 6). Unsupervised CAs based on morphological and/or electrophysiological parameters were performed to allow an objective classification of neurons. To investigate if morphological subtypes also display electrophysiological differences and vice versa, we first performed CAs based only on morphological or on electrophysiological parameters. When we found that these separate analysis procedures led to similar grouping of neurons, we combined morphological and electrophysiological parameters in one CA. We identified between 1 and 4 pyramidal subtypes for each cortical layer. For L3 and L5 pyramidal neurons, a clear correlation between physiological properties and the dendritic morphology of these neurons was found. This enabled us to make a classification based on the combined structural and functional characteristics of these cells. L2 and L6 pyramidal neurons showed no such correlation of structural and functional characteristics, and classifications were based either on active or passive electrophysiological parameters, or morphological parameters.

Layer 2

L2 pyramidal neurons showed no correlation between the electrophysiological and morphological data. This could be due to the fact that these neurons share similar morphological features such as a broad tufted apical dendrites, of which the field span is wider than that of basal dendrites. Hence, potential physiological subtypes would show similar morphologies. Electrophysiologically, L2 pyramidal neurons were also similar. Although individual neurons could show a more RS or a more adapting firing pattern, this was not mirrored in the passive physiological properties. Indeed, all L2 pyramidal neurons had a very hyperpolarized RMP that set them apart from pyramidal neurons of other layers. Thus, when compared with pyramidal cells of other layers L2 neurons appeared to be a rather homogenous neuron class, and small differences in physiological or

morphological parameters do not seem to reflect intrinsically different subtypes. This result may not be surprising considering the small size of L2.

The border between L2 and L3 is remarkably clear in the mPFC. Macroscopically, L2 can be seen as a thin dark band directly below the optically empty L1 (Fig. 1*A*). At the microscopic level, a decrease in cell density can be observed that is characteristic for the border with L3. In the mPFC, L2 is only a thin layer, about a quarter of the size of L3, consisting of only a couple of "rows" of densely packed pyramidal neurons. Physiologically, broad tufted RS L3 pyramidal neurons resembled those in L2 pyramidal neurons to a significant extent, explaining why these 2 subtypes cluster together and only separate at lower cutoff values in the CA (Fig. 5*A*). RS L3 neurons were however unique in their extremely low excitability: the rheobase value for RS L3 neurons was not only different from L2 neurons, but was the highest of all subtypes (Table 3 and Supplementary Table 10). Morphologically, L2 and RS L3 neuron subtypes were very different: L2 neurons possessed a wider apical tree that contained more branches, whereas the basal dendritic tree was more developed in RS L3 neurons (Supplementary Table 10).

Layer 3

L3 pyramidal neurons with adapting firing patterns exhibited either a slender tufted or a broad tufted apical dendrite. This is in marked contrast to L5 pyramidal neurons of the mPFC, where adapting neurons always possessed a slender tufted apical dendrite and broad tufted morphologies exclusively belonged to RS L5 neurons. Electrophysiologically, both types of slender tufted L3 neurons, namely, bursting and adapting neurons, differed from both types of broad tufted neurons, RS and adapting, in the RMP and size of the voltage sag: the broad tufted subtypes had more hyperpolarized RMPs and virtually lacked a voltage sag (Table 5). Therefore, also for electrophysiological properties broad tufted adapting L3 neurons differ more from slender tufted L5 neurons than their slender tufted counterparts. Thus, it is not surprising that slender tufted adapting L3 neurons mixed to some extent with slender tufted L5 neurons in the CA of all pyramidal neurons, whereas broad tufted adapting L3 neurons remained as a separate cluster (Fig. 5). The total dendritic length of both subtypes of slender tufted L5 neuron was significantly larger than that of slender tufted Ad L3 neurons; however, the ratio of basal versus apical dendritic length were comparable for slender tufted Ad L3 and L5-LR neurons (Supplementary Table 11). Thus, slender tufted Ad L3 neurons could be regarded as "down-sized" versions of slender tufted L5-LR neurons: smaller, but with the same shape of the dendritic tree and a similar physiology.

Bursting neurons were found exclusively in L3 and were the only subtype that upon medium current (<300 pA) stimulation responded with a short burst of APs alone. Pyramidal neurons with this electrophysiological profile have been described before as "fast-adapting RS" cells in Degenetais et al. (2002) where 2 of the 3 reconstructed neurons were found in rat prefrontal L2/3. The study by Chang and Luebke (2007) found that 5% of L5 pyramidal neurons in monkey prefrontal cortex showed a similar bursting electrophysiological profile (intrinsic bursting cells). The only "IB" neuron that could be reconstructed however had a very superficial location of its soma at the border of L3–L5. We would therefore hypothesize that their "L5 IB" neurons are in fact similar to the L3 bursting neurons presented in this article.

Layer 5

Prefrontal L5 pyramidal neurons have been described more extensively, and have been categorized according to their electrophysiological or morphological properties, and/or their axonal projection targets. Although some studies combine physiological and morphological analysis of pyramidal neurons subtypes (Dembrow et al. 2010), most studies show only representative examples of the morphology of neurons to accompany their physiological analysis (Yang et al. 1996; Degenetais et al. 2002; Chang and Luebke 2007), or vice versa show an example voltage trace for their defined morphological subtypes (Wang et al. 2006). In our study, an unsupervised CA of electrophysiological and morphological properties identified 3 L5 pyramidal neuron subtypes: 1) broad tufted RS neurons, 2) slender tufted adapting neurons with high cellular R_{in} and sparse basal dendrites (L5-HR), and 3) slender tufted adapting neurons with lower R_{in} and numerous basal dendrites (L5-LR). The main division of broad versus slender tufted and RS versus adapting spiking seems to be in line with previous studies in mPFC (Wang et al. 2006; Dembrow et al. 2010; Avesar and Gulledge 2012).

Previous studies in primary sensory cortices have described the relation between the axonal projection targets and the morphological and physiological properties of L5 pyramidal neurons (Molnar and Cheung 2006; Hattox and Nelson 2007). It has been suggested that L5 pyramidal neurons in the neocortex can be divided in at least 2 subpopulations: 1) "broad" or "thick" tufted pyramidal neurons with long-range corticofugal projections to the brain stem, thalamus, superior colliculus, pons, and trigeminal nucleus and 2) "slender" or "thin" tufted pyramidal neurons that project to the contralateral cortex ("callosal" neurons) or to the striatum. Importantly, not only morphological differences are found between projection types, but also differences in physiological properties and intracortical connectivity (Otsuka and Kawaguchi 2008; Brown and Hestrin 2009).

For the mPFC, differences in morphological and physiological properties have been described for L5 pyramidal neurons that project to the pons (corticopontine, CPn) or to the contralateral cortex (commisural, COM) that match our results (Dembrow et al. 2010). CPn neurons had a lower cellular input resistance, a faster membrane time constant and a larger voltage sag compared with COM neurons. Also, in our dataset, RS L5 neurons differed significantly from both types of adapting L5 neurons in these physiological properties. Likewise, CPn neurons possessed a broad tufted apical dendrite, whereas COM neurons were slender tufted. These similarities in morphological and electrophysiological properties suggest that the broad tufted RS L5 pyramidal neurons we identified may be CPn projecting neurons, and the slender tufted adapting L5 pyramidal neurons may project to the contralateral cortex (Dembrow et al. 2010). Interestingly, in the above quoted study, the observed variation for physiological properties was larger for COM neurons than for CPn neurons, suggesting that the COM-projecting pyramidal neurons may actually consist of both slender tufted subtypes we identified in this study: L5-LR and L5-HR neurons. Gee et al. (2012) used

the amplitude of h-current to distinguish between corticothalamic (CT) and corticocortico (CC) projecting L5 mPFC pyramidal neurons. Similarly, we also found that broad tufted L5 neurons displayed a larger voltage sag, albeit not in the nonoverlapping manner reported in their study. However, in other frontal cortex areas, the correlation between physiological subtype and projection target is not always found to be so clear-cut, especially for L5 pyramidal neurons projecting to the contralateral cortex (Otsuka and Kawaguchi 2008, 2011).

A tripartite division of L5 pyramidal neurons in the frontal cortex has been suggested by Otsuka and Kawaguchi (2008, 2011). Their classification is based solely on the firing pattern of pyramidal neurons and distinguishes RS neurons (slow-adapting) with or without a doublet spike, and adapting neurons (fast-adapting). In our study, such a classification did not lead to clear clusters. We did not observe a clear-cut difference between RS neurons with or without doublets. Instead, the first ISI of RS L5 neurons in our study would display a continuum, suggesting possible regional differences between L5 pyramidal subtypes.

The detailed morphological analysis that we performed showed that the morphology of the basal dendrites is also an important factor distinguishing the 2 subtypes of slender tufted adapting L5 neurons. Apart from the total length and number of branches of basal dendrites, these subtypes also differed in their passive electrophysiological properties displaying significant differences in cell excitability and temporal summation kinetics.

Some studies report subtypes that we did not encounter: "rhythmic oscillatory bursting" neurons and "noninactivating bursting cells" (Yang et al. 1996; Degenetais et al. 2002). As these types are rare (7–13%), we may have missed them despite our relatively large sample size of 65 L5 pyramidal neurons. Another possible explanation could lie in different ages of the test animals or differences of the internal solution used in this and other studies (Staiger et al. 2004). Moreover, noninactivating bursting neurons have thus far been found only in in vivo preparations (Degenetais et al. 2002).

Layer 6

The large morphological diversity of L6 pyramidal neurons makes a correlation with physiological parameters very difficult. L6 has been described previously in other cortical regions as extremely heterogeneous, and this appears to apply also to the mPFC (Tömböl 1984; Valverde et al. 1989; Van Brederode and Snyder 1992; Zhang and Deschenes 1997; Zarrinpar and Callaway 2006; Kumar and Ohana 2008; Thomson 2010; Marx and Feldmeyer 2012; Pichon et al. 2012). Contrary to the morphological diversity, however, L6 pyramidal neurons in the mPFC were unique in their low adaptation rate and high excitability, partly due to their high cellular input resistance (Table 3). Therefore, despite some morphological similarities between tall L6 neurons and slender tufted L5 pyramidal neurons, these pyramidal subtypes differed substantially for several parameters (Supplementary Table 12). We did not observe significant differences in the electrophysiological properties between morphological subtypes as has been described for L6 neurons in the visual cortex (Mercer et al. 2005). However, it will be necessary to increase the number of recorded L6 pyramidal neurons significantly to clearly identify different morphological subtypes and their morphological and electrophysiological characteristics. Indeed, a purely qualitative analysis would classify half of the reconstructed neurons as unique morphologies (Supplementary Fig. 5).

Despite the diversity of L6 pyramidal cell morphologies, it is striking that almost 40% of them have ascending apical dendrites that end in L1. This percentage can be even higher in juvenile mice and seems to be dependent on the developmental switch in nicotinic receptor subunits (Bailey et al. 2012). Although this morphology has been described before in cat and rat visual cortex for "claustrum projection pyramidal neurons," they form only a small fraction (~5% of neurons) in these cortices (Katz 1987; Van Brederode and Snyder 1992; Thomson 2010). For somatosensory cortex, this cell type is not mentioned in the literature, although findings in our laboratory indicate that it is also present, albeit to a significantly smaller degree (~10%, personal observations Drs Robert Günter and Guanxiao Qi). About 40% of L6 pyramidal neurons in the mPFC send their axons to the thalamus, the main projection area of these neurons (Hoover and Vertes 2007). The second and third largest known projection targets are the lateral hypothalamus (11%) and the dorsal striatum (6%) (Hoover and Vertes 2007). However, for an estimated 40% of L6 neurons the projection area is still unknown. Therefore, it is conceivable that tall L6 pyramidal neurons may have different projection targets.

Classification Based on Lineage, Birthday, or Molecular Markers

In the neocortex, cell fate is closely related to cell birthday: Pyramidal neurons in deeper layers are born earlier than pyramidal neurons from upper layers, the so-called inside-out configuration (Angevine and Sidman 1961; Rakic 1974). Several neuronal progenitors have been identified that give rise to pyramidal neurons in upper or deeper layers (Kawaguchi et al. 2008; Leone et al. 2008; Kowalczyk et al. 2009). In recent years, much progress has been made in the identification of specific molecular markers, such as developmental transcription factors, that identify cell lineages (Hevner et al. 2003; Gaspard et al. 2008; Harwell et al. 2012). Thus, specific markers could be used to identify neuronal subpopulations. For example, in the neocortex different markers are expressed among L5 corticofugal and callosal neurons pyramidal neurons (Arlotta et al. 2005; Leone et al. 2008). Further progress in this field of study will help to ultimately classify pyramidal cell types based on cell lineage and molecular markers, as well as axonal projections, neuronal morphology, and electrophysiological properties.

Future Directions

In order to comprehend the functional consequences of the here identified pyramidal subtypes, it would be worthwhile to investigate the specific projection targets of each subtype. Especially for L3 and L6 subtypes, this is at present unexplored. Not only will it be interesting to know if these subtypes project to different regions outside the mPFC, also the intracortical connectivity is largely unknown. Additionally, microarray analysis could be used to identify genes that are expressed in a cell-type-specific way (Sugino et al. 2006; Bernard et al. 2009). Such studies will greatly contribute to our understanding of cortical processing in the mPFC.

Conclusion

Pyramidal neurons in the mPFC are highly heterogeneous. Unsupervised CA of electrophysiological and/or morphological

properties enabled us to identify more than 10 different pyramidal subtypes spread across the different cortical layers.

For future experiments, it is important to consider the exact pyramidal subtypes that are studied. Indeed, for several neuromodulators, it is already known that they affect L5 pyramidal neurons in a subtype-specific way (Beique et al. 2007; Dembrow et al. 2010). This also extends to pyramidal subtypes in L3, which show marked differences in sensitivity to the neuromodulator adenosine (Van Aerde et al. 2013). A detailed knowledge of the role of neuromodulators for pyramidal neuron subtypes throughout the cortical layers of the mPFC could lead to a deepened understanding of cortical processing under various behavioral conditions.

Supplementary Material

Supplementary material can be found at: http://www.cercor.oxfordjournals.org/.

Funding

This work was supported by the Helmholtz Alliance for Systems Biology.

Notes

We thank Werner Hucko for excellent technical assistance and Andreas Kriebel and Liang Dongling for help with morphological reconstructions. We thank Ted Abel (University of Pennsylvania) for his useful comments on this manuscript. *Conflict of Interest*: None declared.

References

Angevine JB Jr, Sidman RL. 1961. Autoradiographic study of cell migration during histogenesis of cerebral cortex in the mouse. Nature. 192:766–768.

Arlotta P, Molyneaux BJ, Chen J, Inoue J, Kominami R, Macklis JD. 2005. Neuronal subtype-specific genes that control corticospinal motor neuron development in vivo. Neuron. 45:207–221.

Avesar D, Gulledge AT. 2012. Selective serotonergic excitation of callosal projection neurons. Front Neural Circuits. 6:12.

Bailey CD, Alves NC, Nashmi R, De Biasi M, Lambe EK. 2012. Nicotinic alpha5 subunits drive developmental changes in the activation and morphology of prefrontal cortex layer VI neurons. Biol Psychiatry. 71:120–128.

Beique JC, Imad M, Mladenovic L, Gingrich JA, Andrade R. 2007. Mechanism of the 5-hydroxytryptamine 2a receptor-mediated facilitation of synaptic activity in prefrontal cortex. Proc Natl Acad Sci USA. 104:9870–9875.

Bernard A, Sorensen SA, Lein ES. 2009. Shifting the paradigm: new approaches for characterizing and classifying neurons. Curr Opin Neurobiol. 19:530–536.

Broersen LM, Heinsbroek RP, De Bruin JP, Uylings HB, Olivier B. 1995. The role of the medial prefrontal cortex of rats in short-term memory functioning: further support for involvement of cholinergic, rather than dopaminergic mechanisms. Brain Res. 674:221–229.

Brown SP, Hestrin S. 2009. Intracortical circuits of pyramidal neurons reflect their long-range axonal targets. Nature. 457:1133–1136.

Chang YM, Luebke JI. 2007. Electrophysiological diversity of layer 5 pyramidal cells in the prefrontal cortex of the rhesus monkey: in vitro slice studies. J Neurophysiol. 98:2622–2632.

Chudasama Y, Passetti F, Rhodes SE, Lopian D, Desai A, Robbins TW. 2003. Dissociable aspects of performance on the 5-choice serial reaction time task following lesions of the dorsal anterior cingulate, infralimbic and orbitofrontal cortex in the rat: differential effects on selectivity, impulsivity and compulsivity. Behav Brain Res. 146:105–119.

Couey JJ, Meredith RM, Spijker S, Poorthuis RB, Smit AB, Brussaard AB, Mansvelder HD. 2007. Distributed network actions by nicotine increase the threshold for spike-timing-dependent plasticity in prefrontal cortex. Neuron. 54:73–87.

Degenetais E, Thierry AM, Glowinski J, Gioanni Y. 2002. Electrophysiological properties of pyramidal neurons in the rat prefrontal cortex: an in vivo intracellular recording study. Cereb Cortex. 12:1–16.

Dembrow NC, Chitwood RA, Johnston D. 2010. Projection-specific neuromodulation of medial prefrontal cortex neurons. J Neurosci. 30:16922–16937.

Douglas RJ, Martin KA. 2004. Neuronal circuits of the neocortex. Annu Rev Neurosci. 27:419–451.

Eggermann E, Feldmeyer D. 2009. Cholinergic filtering in the recurrent excitatory microcircuit of cortical layer 4. Proc Natl Acad Sci USA. 106:11753–11758.

Elston GN. 2003. Cortex, cognition and the cell: new insights into the pyramidal neuron and prefrontal function. Cereb Cortex. 13:1124–1138.

Feldmeyer D. 2012. Excitatory neuronal connectivity in the barrel cortex. Front Neuroanat. 6:24.

Feldmeyer D, Lubke J, Silver RA, Sakmann B. 2002. Synaptic connections between layer 4 spiny neurone-layer 2/3 pyramidal cell pairs in juvenile rat barrel cortex: physiology and anatomy of interlaminar signalling within a cortical column. J Physiol. 538:803–822.

Feldmeyer D, Roth A, Sakmann B. 2005. Monosynaptic connections between pairs of spiny stellate cells in layer 4 and pyramidal cells in layer 5a indicate that lemniscal and paralemniscal afferent pathways converge in the infragranular somatosensory cortex. J Neurosci. 25:3423–3431.

Fuster JM. 2000. Prefrontal neurons in networks of executive memory. Brain Res Bull. 52:331–336.

Fuster JM. 2001. The prefrontal cortex–an update: time is of the essence. Neuron. 30:319–333.

Gabbott PL, Dickie BG, Vaid RR, Headlam AJ, Bacon SJ. 1997. Local-circuit neurons in the medial prefrontal cortex (areas 25, 32 and 24b) in the rat: morphology and quantitative distribution. J Comp Neurol. 377:465–499.

Gabbott PL, Warner TA, Jays PR, Salway P, Busby SJ. 2005. Prefrontal cortex in the rat: projections to subcortical autonomic, motor, and limbic centers. J Comp Neurol. 492:145–177.

Gaspard N, Bouschet T, Hourez R, Dimidschstein J, Naeije G, Van Den Ameele J, Espuny-Camacho I, Herpoel A, Passante L, Schiffmann SN et al. 2008. An intrinsic mechanism of corticogenesis from embryonic stem cells. Nature. 455:351–357.

Gee S, Ellwood I, Patel T, Luongo F, Deisseroth K, Sohal VS. 2012. Synaptic activity unmasks dopamine d2 receptor modulation of a specific class of layer v pyramidal neurons in prefrontal cortex. J Neurosci. 32:4959–4971.

Goldman-Rakic PS. 1995. Cellular basis of working memory. Neuron. 14:477–485.

Harrison Y, Horne JA, Rothwell A. 2000. Prefrontal neuropsychological effects of sleep deprivation in young adults—a model for healthy aging? Sleep. 23:1067–1073.

Harwell CC, Parker PR, Gee SM, Okada A, Mcconnell SK, Kreitzer AC, Kriegstein AR. 2012. Sonic hedgehog expression in corticofugal projection neurons directs cortical microcircuit formation. Neuron. 73:1116–1126.

Hattox AM, Nelson SB. 2007. Layer v neurons in mouse cortex projecting to different targets have distinct physiological properties. J Neurophysiol. 98:3330–3340.

Hevner RF, Daza RA, Rubenstein JL, Stunnenberg H, Olavarria JF, Englund C. 2003. Beyond laminar fate: toward a molecular classification of cortical projection/pyramidal neurons. Dev Neurosci. 25:139–151.

Hooks BM, Hires SA, Zhang YX, Huber D, Petreanu L, Svoboda K, Shepherd GM. 2011. Laminar analysis of excitatory local circuits in vibrissal motor and sensory cortical areas. PLoS Biol. 9:e1000572.

Hoover WB, Vertes RP. 2007. Anatomical analysis of afferent projections to the medial prefrontal cortex in the rat. Brain Struct Funct. 212:149–179.

Katz LC. 1987. Local circuitry of identified projection neurons in cat visual cortex brain slices. J Neurosci. 7:1223–1249.
Kawaguchi A, Ikawa T, Kasukawa T, Ueda HR, Kurimoto K, Saitou M, Matsuzaki F. 2008. Single-cell gene profiling defines differential progenitor subclasses in mammalian neurogenesis. Development. 135:3113–3124.
Killcross S, Coutureau E. 2003. Coordination of actions and habits in the medial prefrontal cortex of rats. Cereb Cortex. 13:400–408.
Kowalczyk T, Pontious A, Englund C, Daza RA, Bedogni F, Hodge R, Attardo A, Bell C, Huttner WB, Hevner RF. 2009. Intermediate neuronal progenitors (basal progenitors) produce pyramidal-projection neurons for all layers of cerebral cortex. Cereb Cortex. 19:2439–2450.
Kumar P, Ohana O. 2008. Inter- and intralaminar subcircuits of excitatory and inhibitory neurons in layer 6a of the rat barrel cortex. J Neurophysiol. 100:1909–1922.
Leone DP, Srinivasan K, Chen B, Alcamo E, Mcconnell SK. 2008. The determination of projection neuron identity in the developing cerebral cortex. Curr Opin Neurobiol. 18:28–35.
Marquis JP, Killcross S, Haddon JE. 2007. Inactivation of the prelimbic, but not infralimbic, prefrontal cortex impairs the contextual control of response conflict in rats. Eur J Neurosci. 25:559–566.
Marx M, Feldmeyer D. 2013. Morphology and physiology of excitatory neurons in layer 6b of the somatosensory rat barrel cortex. Cereb Cortex. 23:2803–2817.
Marx M, Gunter RH, Hucko W, Radnikow G, Feldmeyer D. 2012. Improved biocytin labeling and neuronal 3d reconstruction. Nat Protoc. 7:394–407.
Mercer A, West DC, Morris OT, Kirchhecker S, Kerkhoff JE, Thomson AM. 2005. Excitatory connections made by presynaptic corticocortical pyramidal cells in layer 6 of the neocortex. Cereb Cortex. 15:1485–1496.
Miller EK. 2000. The prefrontal cortex and cognitive control. Nat Rev Neurosci. 1:59–65.
Molnar Z, Cheung AF. 2006. Towards the classification of subpopulations of layer v pyramidal projection neurons. Neurosci Res. 55:105–115.
Murphy ER, Dalley JW, Robbins TW. 2005. Local glutamate receptor antagonism in the rat prefrontal cortex disrupts response inhibition in a visuospatial attentional task. Psychopharmacology (Berl). 179:99–107.
Muzur A, Pace-Schott EF, Hobson JA. 2002. The prefrontal cortex in sleep. Trends Cogn Sci. 6:475–481.
Oberlaender M, De Kock CP, Bruno RM, Ramirez A, Meyer HS, Dercksen VJ, Helmstaedter M, Sakmann B. 2012. Cell type-specific three-dimensional structure of thalamocortical circuits in a column of rat vibrissal cortex. Cereb Cortex. 22:2375–2391.
Otsuka T, Kawaguchi Y. 2011. Cell diversity and connection specificity between callosal projection neurons in the frontal cortex. J Neurosci. 31:3862–3870.
Otsuka T, Kawaguchi Y. 2008. Firing-pattern-dependent specificity of cortical excitatory feed-forward subnetworks. J Neurosci. 28:11186–11195.
Paxinos G, Watson C. 2005. The rat brain in stereotaxic coordinates. San Diego (CA): Academic Press.
Pichon F, Nikonenko I, Kraftsik R, Welker E. 2012. Intracortical connectivity of layer VI pyramidal neurons in the somatosensory cortex of normal and barrelless mice. Eur J Neurosci. 35:855–869.
Poorthuis RB, Bloem B, Schak B, Wester J, De Kock CP, Mansvelder HD. 2013. Layer-specific modulation of the prefrontal cortex by nicotinic acetylcholine receptors. Cereb Cortex. 23:148–161.
Radnikow G, Günter RH, Marx M, Feldmeyer D. 2012. Morphofunctional mapping of cortical networks in brain slice preparations using paired electrophysiological recordings. In: Fellin T, Halassa MM ed. Neural Network Analysis. 1st ed. Berlin (Germany): Springer Verlag. p 405–431.
Ragozzino M. 2007. The contribution of the medial prefrontal cortex, orbitofrontal cortex and dorsomedial striatum to behavioral flexibility. Ann NY Acad Sci. 1121:355–375.
Rakic P. 1974. Neurons in rhesus monkey visual cortex: systematic relation between time of origin and eventual disposition. Science. 183:425–427.
Schubert D, Kotter R, Luhmann HJ, Staiger JF. 2006. Morphology, electrophysiology and functional input connectivity of pyramidal neurons characterizes a genuine layer va in the primary somatosensory cortex. Cereb Cortex. 16:223–236.
Schubert D, Kotter R, Staiger JF. 2007. Mapping functional connectivity in barrel-related columns reveals layer- and cell type-specific microcircuits. Brain Struct Funct. 212:107–119.
Shepherd GM. 2009. Intracortical cartography in an agranular area. Front Neurosci. 3:337–343.
Staiger JF, Flagmeyer I, Schubert D, Zilles K, Kotter R, Luhmann HJ. 2004. Functional diversity of layer iv spiny neurons in rat somatosensory cortex: quantitative morphology of electrophysiologically characterized and biocytin labeled cells. Cereb Cortex. 14:690–701.
Sugino K, Hempel CM, Miller MN, Hattox AM, Shapiro P, Wu C, Huang ZJ, Nelson SB. 2006. Molecular taxonomy of major neuronal classes in the adult mouse forebrain. Nat Neurosci. 9:99–107.
Thomson AM. 2010. Neocortical layer 6, a review. Front Neuroanat. 4:13.
Thorndike RL. 1953. Who belongs in the family? Psychometrika. 18:267–276.
Tömböl T. 1984. Layer VI cells. In: Peters A, Jones EG ed. Cerebral Cortex. 1st ed. London (United Kingdom): Plenum Press. p. 479–510.
Uylings HB, Groenewegen HJ, Kolb B. 2003. Do rats have a prefrontal cortex? Behav Brain Res. 146:3–17.
Uylings HB, Van Eden CG. 1990. Qualitative and quantitative comparison of the prefrontal cortex in rat and in primates, including humans. Prog Brain Res. 85:31–62.
Valverde F, Facal-Valverde MV, Santacana M, Heredia M. 1989. Development and differentiation of early generated cells of sublayer vib in the somatosensory cortex of the rat: a correlated golgi and autoradiographic study. J Comp Neurol. 290:118–140.
Van Aerde KI, Qi G, Feldmeyer D. 2015. Cell-type specific effects of adenosine on cortical neurons. Cereb Cortex. 25:772–787.
Van Brederode JF, Snyder GL. 1992. A comparison of the electrophysiological properties of morphologically identified cells in layers 5b and 6 of the rat neocortex. Neuroscience. 50:315–337.
Van Der Werf YD, Altena E, Schoonheim MM, Sanz-Arigita EJ, Vis JC, De Rijke W, Van Someren EJ. 2009. Sleep benefits subsequent hippocampal functioning. Nat Neurosci. 12:122–123.
Van Eden CG, Uylings HB. 1985. Cytoarchitectonic development of the prefrontal cortex in the rat. J Comp Neurol. 241:253–267.
Wang Y, Markram H, Goodman PH, Berger TK, Ma J, Goldman-Rakic PS. 2006. Heterogeneity in the pyramidal network of the medial prefrontal cortex. Nat Neurosci. 9:534–542.
Yang CR, Seamans JK, Gorelova N. 1999. Developing a neuronal model for the pathophysiology of schizophrenia based on the nature of electrophysiological actions of dopamine in the prefrontal cortex. Neuropsychopharmacology. 21:161–194.
Yang CR, Seamans JK, Gorelova N. 1996. Electrophysiological and morphological properties of layers v-vi principal pyramidal cells in rat prefrontal cortex in vitro. J Neurosci. 16:1904–1921.
Zarrinpar A, Callaway EM. 2006. Local connections to specific types of layer 6 neurons in the rat visual cortex. J Neurophysiol. 95: 1751–1761.
Zhang ZW, Deschenes M. 1997. Intracortical axonal projections of lamina vi cells of the primary somatosensory cortex in the rat: a single-cell labeling study. J Neurosci. 17:6365–6379.